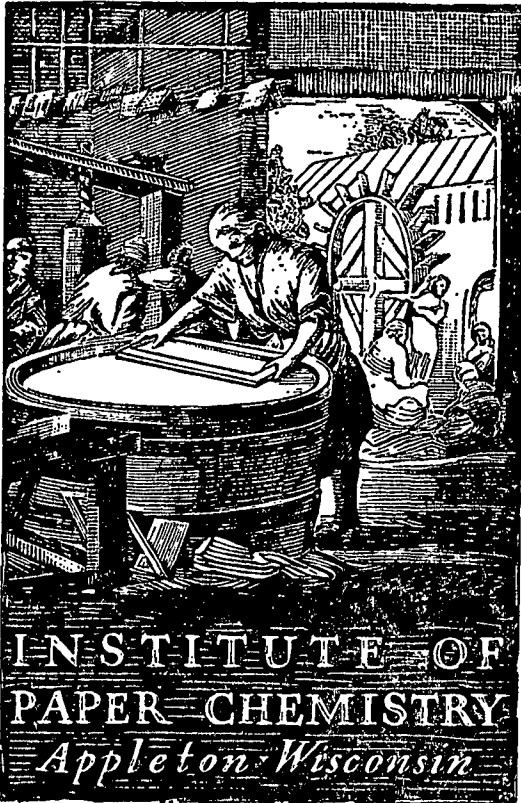


2348
#6



STUDIES OF THE SHEET-FORMING PROCESS

**Hydrodynamic Fiber-Wire Interaction of
Thin Wood-Fiber Mats**

Project 2348

Report Six

A Progress Report

to

MEMBERS OF GROUP PROJECT 2348

July 16, 1964

THE INSTITUTE OF PAPER CHEMISTRY
Appleton, Wisconsin

STUDIES OF THE SHEET-FORMING PROCESS
HYDRODYNAMIC FIBER-WIRE INTERACTION OF THIN WOOD-FIBER MATS

Project 2348

Report Six
A Progress Report
to

MEMBERS OF GROUP PROJECT 2348

July 16, 1964

Members of Group Project 2348:

Consolidated Papers, Inc.

Crown Zellerbach Corporation

Eastman Kodak Company

The Eaton-Dikeman Company

P. H. Glatfelter Co.

International Paper Company

Kimberly-Clark Corporation

KVP Sutherland Paper Company

Longview Fibre Company

Marathon, A Division of American Can Company

The Mead Corporation

Personal Products Company

Riegel Paper Corporation

St. Regis Paper Company

Scott Paper Company

Union Bag-Camp Paper Corporation

West Virginia Pulp and Paper Company

TABLE OF CONTENTS

	Page
SUMMARY	1
INTRODUCTION	3
SEPARATION OF MAT RESISTANCE FROM A COMPOSITE MAT-WIRE RESISTANCE	6
FLOW RESISTANCE AND SMALL UPSTREAM DISTURBANCES	7
LAMINAR FLOW THROUGH FIBER MAT AND SUPPORTING WIRE	9
FIBER MAT UPON LINEAR ARRAY OF CYLINDERS	12
APPLICATIONS TO TWO DEFINED MAT CROSS SECTIONS	19
APPLICATION TO EXPERIMENTS	29
DISCUSSION OF RESULTS AND CONCLUSIONS	43
NOMENCLATURE	46
ACKNOWLEDGMENT	48
LITERATURE CITED	48
APPENDIX I. ON THE NUMERICAL SEPARABILITY OF VISCOUS AND INERTIAL TERMS OF THE FORCHHEIMER EQUATION BY MEANS OF ONE SET OF EXPERIMENTAL DATA	49

THE INSTITUTE OF PAPER CHEMISTRY
Appleton, Wisconsin

STUDIES OF THE SHEET-FORMING PROCESS

HYDRODYNAMIC FIBER-WIRE INTERACTION OF THIN WOOD-FIBER MATS

SUMMARY

The two problems of determining the effect of flow convergence on the pressure drop across a fiber mat and the numerical separation of the fiber mat resistance from the compound mat-wire resistance are found to be interrelated. In view of the negligible effect of small disturbances on the boundary layer flow of obstacle spheres and circular cylinders in the subcritical range of flow, it is assumed that the individual fibers of a fiber mat resemble such disturbances, and it is shown by discussion of a resulting inhomogeneous Laplace equation that the standard separation equation would be compatible only for a homogeneous and incompressible mat on top of a wire. For this case and a plane array of cylinders, a solution is communicated and evaluated for two different types of draping mats. The resulting flow convergence factors vary with the porosity of the array, the basis weight of the mat, and the depth of mat penetration into the wire structure. The corrections are significant only for thin mats of usual industrial range and appear to be of the expected magnitude. An attempt was therefore made to find the prediction confirmed by experiments with thin wood fiber mats in the 10 to 80-g./m.² range, each on 65 and 100-mesh wire. Changing fiber specific volume and surface are taken into account, and the method for providing these values from thick and thin mat data are presented. The refined pressure drop predictions follow the tendency as expected from the effect of flow convergence; however, they would require corrections somewhat greater than predicted by theory. It appears that fiber specific volume would depend on both applied stress and a basis-weight-dependent parameter for which a relationship remains to be established by future

experiments. Likewise, more information must be gathered for the compression response of thin mats. In Appendix I, a rigorous proof is given that, in the transition range of flow, experimental data and Forchheimer equation represent an insufficient system of two equations for calculating in one operation both specific volume and surface.

INTRODUCTION

The specialized differential forms of the Darcy and Forchheimer equations,

$$dp/d(W/A) = a_0 U \quad (\text{Darcy}) \quad (1)$$

and

$$dp/d(W/A) = a_0 U + b_0 U^2 \quad (\text{Forchheimer}) \quad (2),$$

where

$\underline{dp/d(W/A)}$ = gradient of piezometric pressure with respect to basis weight,

$\underline{W/A}$ = basis weight,

$\underline{a_0}, \underline{b_0}$ = viscous and inertial resistivities of the fibrous mat on a weight basis, and

\underline{U} = superficial velocity of water within the mat or rate of approach flow per unit area of mat,

which represent the basic formal concepts in the evaluation of filtration and dynamic drainage data, predict the pressure gradient in homogeneous systems at essentially single-component flow. A very thick fibrous mat on top of an ordinary paper machine wire may be considered as an approximately homogeneous system and, with the negligible exception of the immediate vicinity of the wire, the streamlines of the flow will, disregarding small deviations caused by individual fibers, be parallel to the normal of the plane of the wire. In the case of very thin mats, however, the effect of shute and warp wires on the flow through the mat may no longer be disregarded. The wires cause the upstream streamlines to converge, and the entire fiber mat may be exposed to an essentially three-dimensional flow. Flow convergence is seen as one of the major causes of difficulties encountered in correlating thin mat experimental data by means of essentially one-dimensional equations.

The condition of the homogeneity of the system is an implicit one and results from the form of the resistivity coefficients in these equations. These are functions of the mat porosity, specific volume, and specific surface of the fibers only. However, pressure drop measurements can, for obvious reasons, be made only with either composite systems of fiber mats plus supporting wire screen (resulting in total pressure drops, ΔP , as a function of basis weight of the mat and rate of flow) or bare wires [yielding $(\Delta P_w)_0$ as a function of flow rate]. According to the standard procedure adopted in previous work connected with the sheet-forming project (1), it was assumed that reliable pressure drops across the mat, ΔP , could be obtained by simple reduction, namely from

$$\Delta P = \Delta P_{tot} - (\Delta P_w)_0 \quad (3).$$

Apparently, the possible error involved in such a procedure is negligible provided $\Delta P_{tot} \gg (\Delta P_w)_0$, as is generally true in thick mat work. In thin mat filtration, however, which is the domain of industrial papermaking and where ΔP might become of the order of magnitude of $(\Delta P_w)_0$ or less, this procedure needs to be shown to be justified from a hydrodynamic point of view.

Corroborating evidence of, at least, a first-approximation yield of the combined Equations (2) and (3) was furnished by Ingmanson and Andrews in their work on the formation of thin mats of synthetic fibers (1). The majority of their data points scatter about the correlation within a zone of deviation of $\pm 15\%$. It was clearly pointed out that fiber-wire interactions, in particular flow convergence and peculiar changes in the porosity distribution in thin mats, could account for the observed discrepancies. In the same authors' work on thin mats of wood pulp fibers (2), the difficulties encountered in matching experimental data and prediction were considerably greater, as was expected in view of the greater flexibility

and irregular and varying cross sections of the fibers. Based on the observation that some of their thin mats were hardly more than 2 to 12 fiber diameters thick, Ingmanson and Andrews made the assumption that thin wood pulp mats would, depending on the actual basis weight, be compressed more uniformly by fluid stress than would a comparatively thick mat. They introduced a so-called porosity distribution factor which, by calculations with a few data points, could be obtained as a function of basis weight. The general application of this empirical function led, within the range of demonstration, to a very satisfactory agreement between data and prediction. It has been emphasized, however, that force-fitting of the data by an empirical porosity distribution function alone would be unsatisfactory in view of the fact that such a procedure disregards, besides other possible phenomena, the physical fact of flow convergence due to the presence of the supporting wire (2).

It will be shown in the following sections that an approximate investigation into the problem of hydrodynamic compatibility of Equation (3) will, for a simplified case, lead to a prediction of the flow convergence effect upon thin mat data.

SEPARATION OF MAT RESISTANCE FROM A COMPOSITE MAT-WIRE RESISTANCE

The validity of the Equations (1) and (2) in cases where they actually apply is, of course, well established. Notwithstanding the simplicity of its statement, the same cannot immediately be said of Equation (3). On the contrary, it appears to contradict the common experience that the whole is different from the sum of its parts. Its successful application in thin mat work, however, suggests investigation into the conditions under which Equation (3) might actually hold. If it is to be true that a portion of the composite pressure drop which is due to the wire is the same regardless of whether or not a fiber mat is present, there are two main conditions which must be fulfilled:

1. Since the flow resistance of the forming wire results from both skin friction and form drag at and in the wake of individual shute and warp wires, the presence of the mat must neither change the average individual boundary layer thickness nor the average location of flow separation at the individual wires.

2. With the thickness of the individual boundary layers greatly dependent upon the velocity of the surrounding flow, the latter ought to be essentially the same with and without a fiber mat present.

FLOW RESISTANCE AND SMALL UPSTREAM DISTURBANCES

Microphotographs of thin mats on top of forming wires (1) illustrate that the representative diameters of the fibers are usually small as compared with the diameter of the wires, that the surface fraction of the wire which is in actual contact with the fiber is very small, and also that the porosity of thin mat structures may be considerably higher than that of the wire. This image may lead to the tentative conclusion that in the case of flow through such a system, the individual fibers would produce only relatively sporadic wakes of short extension with little over-all effect on the boundary-layer flow around individual wires.

The flow resistance of spheres, which share with circular cylinders a sudden drop of their drag coefficient in the so-called critical range of Reynolds numbers between $Re = 1.5 \times 10^5$ and 4.0×10^5 , has been extensively studied under various conditions of disturbances as caused by suspending and tripping wires, wire screens, and circular rods in various positions of the sphere surface, e.g. (3). Roughly, these investigations showed that small-scale disturbances of the approach flow as produced by the various built-ins would cause the drop of the drag coefficient to shift toward the lower Re number if the approach flow was in a laminar condition. As is well known, the sudden drop itself is the result of a decreasing form drag as the consequence of postponed separation of flow from the sphere. The zone of flow separation shifts behind the sphere equator when the boundary layer becomes turbulent, and it is the flow disturbances from the built-ins which cause this transition to occur at the lower Reynolds number, whereas it occurs at the higher Reynolds number in the absence of these disturbances.

It is now of particular interest to note that disturbances of this kind have no noticeable effect upon the flow resistance of a sphere when subject to subcritical flow (i.e., $Re < 1.5 \times 10^5$). In view of the close similarity

between the drag coefficients for spheres and circular cylinders, it may, for want of direct evidence from the literature, be surmised that an analogous situation will prevail also for the latter.

A paper machine wire is made of cylindrical shute and warp wires which are, relative to the main direction of an approaching flow, in a periodically changing yawed position in addition to periodically overshuting each other. Flow through such a screen has an extremely complicated pattern, but it can be seen that a substantial part of it, namely the component in the direction of the radii of the yaw curvature of the wires, is related to the flow about the cylinders. It is this resemblance and the ordinarily subcritical range of operation which suggest tentatively applying the above conclusions also to paper machine wires. It would mean that the individual fibers of a thin mat would not noticeably disturb the boundary layer flow of the wire. It remains then to be shown whether or not the presence of the fiber mat would alter the flow outside the boundary layers, i.e. the interstitial flow through the wire.

LAMINAR FLOW THROUGH FIBER MAT AND SUPPORTING WIRE

For obvious reasons, it is presently impossible to obtain an exact picture of the flow through a bare wire. In principle, however, flow through a wire would exhibit the same general features as flow around any other obstacle, namely, boundary layers at the individual wires and essentially irrotational interstitial flow. Between the frontal points of stagnation on the wires and those of largest contraction of the interstices, the flow is rapidly accelerated. Consequently, the boundary layers will be very thin in that zone. A knowledge of potential flow through the wire would therefore represent a good approximation of the real flow, including the upstream vicinity of the wire. Assuming a Cartesian co-ordinate system \underline{x} , \underline{y} , \underline{z} with \underline{u} , \underline{v} , \underline{w} as the velocity components in these directions, the latter may be expressed in terms of the velocity potential

$\phi = \phi(\underline{x}, \underline{y}, \underline{z})$ as

$$u = \frac{\partial \phi}{\partial x} ; \quad v = \frac{\partial \phi}{\partial y} ; \quad w = \frac{\partial \phi}{\partial z} \quad (4)$$

Upon introduction of the velocity components (4) into the continuity equation for incompressible fluids,

$$\frac{\partial u}{\partial x} + \frac{\partial v}{\partial y} + \frac{\partial w}{\partial z} = 0 \quad (5)$$

the latter transforms into the Laplace equation,

$$\nabla^2 \phi = \frac{\partial^2 \phi}{\partial x^2} + \frac{\partial^2 \phi}{\partial y^2} + \frac{\partial^2 \phi}{\partial z^2} = 0 \quad (6)$$

At the fixed boundaries, that is, at the cylindrical surface of the wires, the fluid cannot penetrate. Thus, the velocity of the fluid particles can only have the direction perpendicular to the surface normals of general

direction \underline{n} . Since this must include all three velocity components, the condition of impermeability of the walls can be expressed as

$$u \frac{\partial x}{\partial n} + v \frac{\partial y}{\partial n} + w \frac{\partial z}{\partial n} = 0 \quad (7),$$

where the partial derivatives are the direction cosines of the normal. The direction \underline{n} of the normals to the surface is defined only if the geometry of the wire has been fully described, in which case the equation of the wire surface, $S(\underline{x}, \underline{y}, \underline{z}) = 0$, is also known. Then Equation (7) may be replaced by (4)

$$u \frac{\partial S}{\partial x} + v \frac{\partial S}{\partial y} + w \frac{\partial S}{\partial z} = 0 \quad (8).$$

In proceeding at this point to the main problem, namely, whether or not a fibrous mat in the immediate upstream vicinity of the wire would produce a subsequent flow through the wire different from that of the bare wire, we must now prepare the equations of flow through the mat.

In restricting ourselves to laminar flow through the mat, we have, considering three-dimensional flow in the $\underline{x}, \underline{y}, \underline{z}$ space, the velocity components

$$u = -\left(\frac{1}{a}\right) \frac{\partial h}{\partial x} \quad (9),$$

$$v = -\left(\frac{1}{a}\right) \frac{\partial h}{\partial y} \quad (9a),$$

$$w = -\left(\frac{1}{a}\right) \frac{\partial h}{\partial z} \quad (9b),$$

where the resistivity \underline{a} may vary within the mat, in which case $\underline{a} = \underline{a}(\underline{x}, \underline{y}, \underline{z})$ and where the piezometric head, \underline{h} , is a potential. Flow through the mat has to satisfy the continuity Equation (5), and introduction of the above velocity components into the latter yields

$$\nabla^2 h = \frac{\partial^2 h}{\partial x^2} + \frac{\partial^2 h}{\partial y^2} + \frac{\partial^2 h}{\partial z^2} = \frac{1}{a} \left(\frac{\partial a}{\partial x} \frac{\partial h}{\partial x} + \frac{\partial a}{\partial y} \frac{\partial h}{\partial y} + \frac{\partial a}{\partial z} \frac{\partial h}{\partial z} \right) \quad (10).$$

Provided the origin of the Cartesian co-ordinates is the same as that applied in the case of the bare wire, a solution to Equation (10) has to satisfy exactly the same boundary condition (7) and (8), respectively.

In the case of an incompressible homogeneous mat where the resistivity is constant, the individual right-side terms of Equation (10) become zero. This would then mean that the derivatives of the head and velocity potential, h and ϕ , respectively, would differ from each other only by a constant factor ($1/a$) and Equation (10) for the incompressible mat, and Equation (6) for the bare wire thus become identical. Hence, in the presence of an incompressible, homogeneous mat on top of a wire, the pattern of irrotational flow through the subsequent wire does not change. Including our findings regarding the boundary layers at the warp and shute wires, we may, within the limitations of our reasoning, say that Equation (3) holds for viscous flow through incompressible, homogeneous, fibrous mats.

The identity of the two flow equations is lost when Equation (10) applies in full, which is the case for compressible, inhomogeneous mats. This means that the pattern of flow through the composite fiber-wire system is different from that of the bare wire so that the separation of the pressure drops by use of Equation (3) could be in error. In view of the complexity of the structures involved, it appears to be hopeless at the present time to derive an estimate of this error.

However, there is evidence from both papermaking and laboratory practice that thin, fibrous mats yield to fluid stress by deflection as a whole into the wire space rather than by appreciably changing their density, and thus their resistivity. For this reason, it appears to be useful to proceed to a simplified case which, thanks to the existence of a solution, can be treated rigorously.

FIBER MAT UPON LINEAR ARRAY OF CYLINDERS

In the foregoing section it was possible to give some clues regarding the separation Equation (3) without actually solving the flow equations involved. The study of the effect of flow convergence on the mat flow resistance, however, requires solution of the equations. Since no three-dimensional solutions of relevance are known, the two-dimensional case of a mat on top of a linear array of cylinders will be treated. For an x, y co-ordinate system, whose origin will be identified later, we have, provided there is laminar flow through the mat, the system of equations:

$$u = -\left(\frac{1}{a}\right) \frac{\partial h}{\partial x} \quad (11a),$$

$$v = -\left(\frac{1}{a}\right) \frac{\partial h}{\partial y} \quad (11b),$$

$$\frac{\partial u}{\partial x} + \frac{\partial v}{\partial y} = 0 \quad (12).$$

By introduction of the familiar stream function ψ , such that

$$u = \frac{\partial \psi}{\partial y}; \quad v = -\frac{\partial \psi}{\partial x} \quad (13a, b),$$

the continuity equation is identically integrated, and after eliminating the piezometric head, the first two Equations (11a, b) transform into

$$\nabla^2 \psi = \frac{\partial^2 \psi}{\partial x^2} + \frac{\partial^2 \psi}{\partial y^2} = \frac{1}{a} \left(\frac{\partial a}{\partial x} \frac{\partial \psi}{\partial x} + \frac{\partial a}{\partial y} \frac{\partial \psi}{\partial y} \right) \quad (14).$$

The vorticity at a point x, y is given by

$$\xi = \frac{\partial v}{\partial x} - \frac{\partial u}{\partial y} \quad (15),$$

and it can easily be verified that the right side of Equation (14) can be expressed as

$$\frac{1}{a} \left(\frac{\partial a}{\partial x} \frac{\partial \psi}{\partial x} + \frac{\partial a}{\partial y} \frac{\partial \psi}{\partial y} \right) = a \zeta \quad (16).$$

Thus, inhomogeneity of the mat as characterized by varying resistivity, a , causes the flow to become rotational. Generally speaking, the velocity distributions as resulting from the equations for rotational and irrotational flow are not identical.

In the case of negligible changes of resistivity, which would make $\zeta \sim 0$, flow through the mat becomes essentially irrotational, and we have, instead of Equation (14),

$$\nabla^2 \psi = 0 \quad (\text{mat}) \quad (17).$$

Irrotational flow through an array of cylinders is characterized by zero vorticity, $\zeta = 0$, and by use of the Equations (13a, b), Equation (15) assumes the form

$$\nabla^2 \psi = 0 \quad (\text{array}) \quad (18).$$

The boundary condition in terms of ψ may be obtained from Equation (7) with the third term omitted. Replacing the normal element dn by that of the circumference of the cylinders $ds = (dx^2 + dy^2)^{1/2}$, we have, when θ represents the angle between the normal to the surface and the x axis, the relationships

$$\left. \begin{aligned} \cos\theta &= \frac{\partial x}{\partial n} = \frac{\partial y}{\partial s} \\ \sin\theta &= -\frac{\partial y}{\partial n} = \frac{\partial x}{\partial s} \end{aligned} \right\} \quad (19a, b).$$

With \underline{u} and \underline{v} given by the Equations (13a) and (13b), one finds the familiar condition

$$\frac{\partial \psi}{\partial x} \frac{\partial x}{\partial s} + \frac{\partial \psi}{\partial y} \frac{\partial y}{\partial s} = \frac{d\psi}{ds} = 0 \quad (20)$$

around each cylinder. Again flow through the mat is bound by the same condition.

For the situation according to Fig. 1, with \underline{R} = radius of the cylinders, \underline{d} = pitch of the array, \underline{U} = flow velocity at $\underline{x} = -\infty$, and in the direction of the positive \underline{x} axis and with the origin of the \underline{x} , \underline{y} co-ordinate system at the center of one of the cylinders, a solution to Equations (18) and (20) is given by (5):

$$\psi(x, y) = U \left(y - \frac{d}{\pi} \sinh^2 \frac{\pi R}{d} \frac{\sin \frac{2\pi y}{d}}{\cosh \frac{2\pi x}{d} - \cos \frac{2\pi y}{d}} \right) \quad (21).$$

With the centers of the cylinders located at

$$y(0) = 2k \frac{d}{2}; \quad (k = \dots -3, -2, -1, 0, 1, 2, 3\dots) \quad (22),$$

it may be seen that the center lines between two adjacent cylinders,

$$y = (2k + 1) \frac{d}{2} \quad (23),$$

represent streamlines parallel to the \underline{x} axis. Both Equations (22) and (23) are thus lines of symmetry, and it suffices to evaluate the stream function (21) in the range $0 \leq y \leq d/2$.

Equation (21) shows that the streamline $\psi = 0$ consists partly of the \underline{x} axis and partly of a contour whose equation is given by

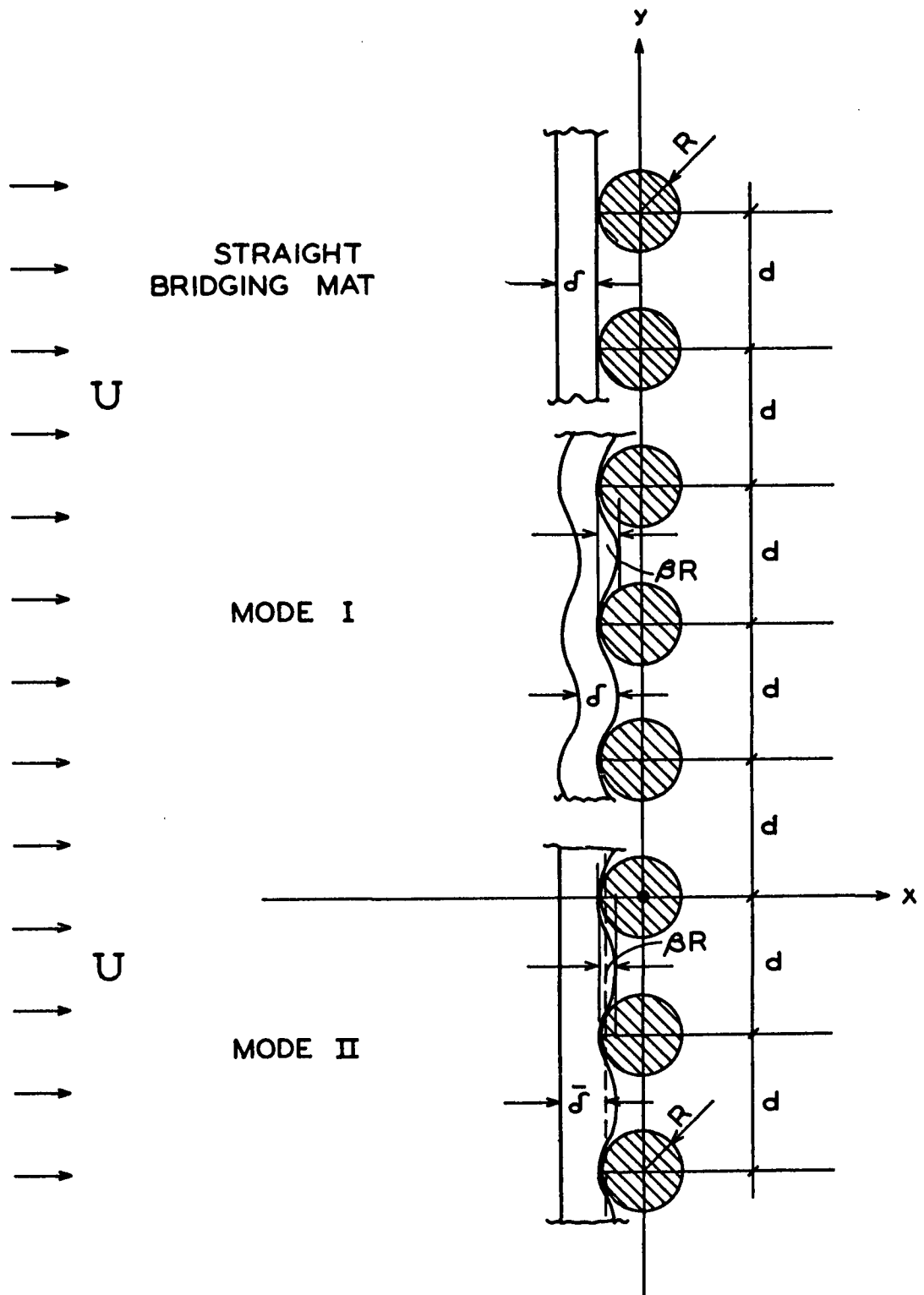


Figure 1. x, y Co-ordinate System and Fiber Mat Models

$$y(x) \left(\cosh \frac{2\tau x}{d} - \cos \frac{2\tau y(x)}{d} \right) - \frac{d}{r} \sinh^2 \frac{\tau R}{d} \sin \frac{2\tau y(x)}{d} = 0 \quad (24).$$

Obviously, the ovality of the contours depends on the radius-to-pitch ratio, $\underline{R/d}$, as shown in Fig. 2 where some solutions of Equation (24) are represented and compared with circular cylinders. As may be seen, the approximation of circular cylinders becomes increasingly better with decreasing ratio $\underline{R/d}$. This peculiarity of the solution (21) has to do with its derivation, which need not concern us here in detail.

It will be desirable to apply Equation (21) in an $\underline{R/d}$ or porosity range which would be equal to that of real forming wires. The porosity, ϵ , of an array of circular cylinders is, using the present nomenclature, given by

$$\epsilon = 1 - \frac{\tau}{2} \frac{R}{d} \quad (25).$$

Thus, assuming $\epsilon = 0.65$ as an average value for a forming wire (6) would require choosing the radius-to-pitch ratio of the array as $\underline{R/d} = 0.223$, which, as may be seen from Fig. 2, is in the range of good approximation of circular cylinders.

Due to the identity of equations and boundary conditions, Equation (21) also represents the solution to Equations (17) and (20), thus describing flow through the mat as caused by the downstream presence of the cylinder array.

The application of the prepared equations to the effect of flow convergence may be outlined as follows. With $\underline{a_0} = \text{constant}$, Equation (1) from the Introduction can be integrated, which, after expressing the pressure drop Δp in terms of the head loss, Δh , and the basis weight, $\underline{W/A}$, in terms of over-all mat thickness, $\underline{\delta}$, may yield

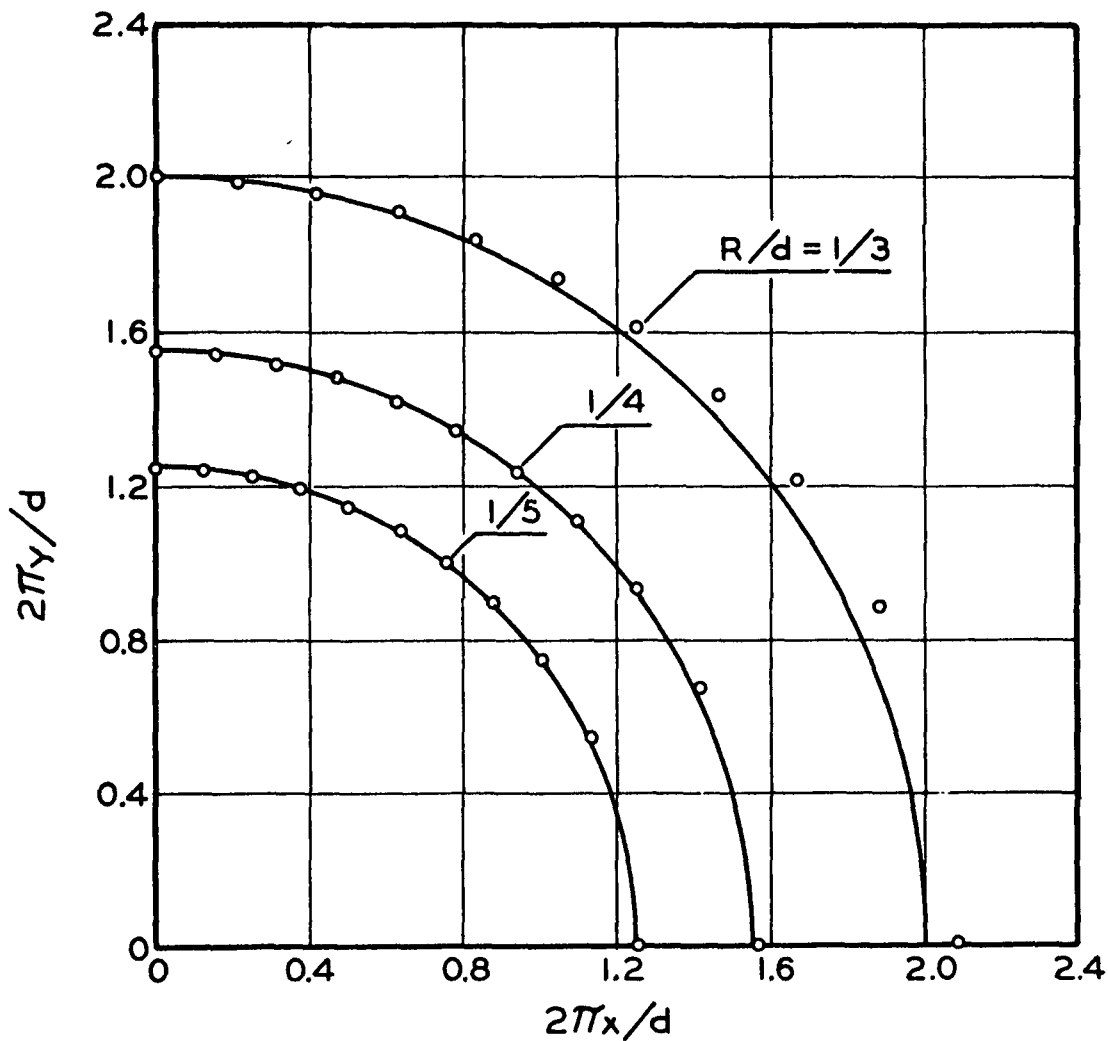


Figure 2. Ovality of Cylindrical Contours as a Function of the Radius-to-Pitch Ratio R/d . [Curves = circles; o = points of solutions of Equation (24)]

$$U = \left(\frac{1}{a}\right) \frac{\Delta h}{\rho} \quad (26).$$

In the case of a thin mat on top of a wire, we expect the apparent filter or superficial velocity \underline{U} no longer to be the effective one unless it results as such from the available system of equations. With the \underline{u} component of mat flow known from Equations (13a) and (21), one obtains by Equation (11a)

$$\begin{aligned} -u(x, y) &= \left(\frac{1}{a}\right) \frac{\partial h}{\partial x} = -U \left[1 - 2 \sinh^2 \frac{rR}{d} f(x, y)\right] \\ f(x, y) &= \frac{\cosh \frac{2rx}{d} \cdot \cos \frac{2ry}{d} - 1}{\left(\cosh \frac{2rx}{d} - \cos \frac{2ry}{d}\right)^2} \end{aligned} \quad (27).$$

This is a partial differential equation, and in order to fully describe the problem a boundary condition is needed, which may be simply stated as

$$h = h_0 \quad \text{at} \quad x = x_0 \quad (28),$$

where x_0 = co-ordinate of the upstream mat face, and where h_0 may be a function of y . Equation (27) must be reduced by proper integrations to a form comparable to Equation (26) in order to determine the effective velocity at converging flow.

APPLICATIONS TO TWO DEFINED MAT CROSS SECTIONS

Before entering into the integration of Equation (27), it is necessary to consider the shape of the space occupied by the mat. Since a mat is formed by depositing one fiber pretty much after another, they will, as a result of fluid drag forces, deflect into the wire space, a well-known fact in papermaking. Two mat space models will be considered in some detail. Both will include, as a special case, a straight mat space which might result from very long and inflexible fibers.

In the first model, the thin mat as a whole is assumed to partially conform to or drape over the individual cylinders of the array. It simulates a mat of apparently uniform mass distribution with imprinted wire mark and will be referred to as Mode I. In the second model the upstream face of the mat is assumed to be planar, i.e., with its trace parallel to the y axis of the co-ordinate system, while its downstream face partially drapes over the cylinders, thus simulating a mat of nonuniform mass distribution. It will be referred to as Mode II. Both modes and their geometric parameters are indicated in Fig. 1.

For want of numerical information on the flexibility of papermaking fibers and in order to avoid (at least for the time being) a more involved study of the deflection of individual fibers under fluid stress and intricate conditions of support, the deflection contour of a mat layer may be approximated by

$$\Delta x = \beta R \sin^2(\tau y/d) ; \quad (0 \leq \beta \leq \beta_1) \quad (29)$$

with a maximum deflection, βR , at the center line between adjacent cylinders, where $y = d/2$, etc. The parameter β may be varied within a certain range whose upper limit, β_1 , is fixed by a surface portion of the cylinders which bounds fiber deflection. It could be shown that

$$\beta_1 \approx 1/2 \pi^2 (R/d)^2 \quad (30)$$

Regardless of the degree of mat deflection, the mat is in contact with the cylinders at the points ($\underline{x} = -R; \underline{y} = 0, d, 2d, \dots$). Upon expressing the mat thickness f , in terms of the cylinder radius R and a measure number, $\alpha > 1$, i.e., by

$$f = (\alpha - 1)R \quad (31)$$

and taking into account mat deflection as expressed by Equation (29), the equations of the upstream and downstream surfaces of a Mode I mat may be found to be

$$x_0 = -R[\alpha - \beta \sin^2(\pi y/d)] \quad (32)$$

and

$$x_1 = -R[1 - \beta \sin^2(\pi y/d)] \quad (33)$$

respectively. With ξ as an auxiliary mat thickness co-ordinate, the running \underline{x} co-ordinate may be expressed as

$$x = R \{ (\alpha - 1)\xi - [\alpha - \beta \sin^2(\pi y/d)] \} \quad (34)$$

so that

$$\partial x = R(\alpha - 1)\partial \xi = f \partial \xi \quad (35)$$

It is advantageous to introduce new independent variables \underline{X} and \underline{Y} according to

$$\frac{2\pi R}{d} (\alpha - 1)\xi = X \quad (36)$$

with

$$\partial \xi = \frac{d}{2\pi R(\alpha - 1)} \partial X \quad (37)$$

and

$$\frac{2\pi y}{d} = Y \quad (38),$$

with

$$dy = \frac{d}{2\pi} dY \quad (39),$$

so that now

$$\partial x = \frac{d}{2\pi} \partial X \quad (40).$$

The ranges of the new variables reduce to

$$0 \leq X \leq X_1 = \frac{2\pi R}{d} (\alpha - 1) \quad (41)$$

and

$$0 \leq Y \leq \pi \quad (42),$$

and the differential Equation (27) assumes the form

$$\left. \begin{aligned} u(x, y) &= -\left(\frac{1}{a}\right) \frac{\partial h}{\partial X} = \frac{d}{2\pi} U[1 - 2\sinh^2(\gamma/2)F(X, Y)] \\ F &= \frac{\cosh(X - \gamma[\alpha - \beta \sin^2(Y/2)]) \cos Y - 1}{\{\cosh(X - \gamma[\alpha - \beta \sin^2(Y/2)]) - \cos Y\}^2} \\ \gamma &= \frac{2\pi R}{d} \end{aligned} \right\} (43).$$

Upon integration over the X range as given by (41), one obtains, observing the boundary condition (28),

$$\left. \left(\frac{1}{a} \right) \frac{h_o(y) - h_1(y)}{\delta} = U \omega_I(y) \right\} \quad (44),$$

with

$$\omega_I(y) = 1 - \frac{2 \sinh^2(\gamma/2)}{X_1} \int_0^{X_1} F(X, Y) dX$$

and where the subscript I refers to the Mode I deflection of the mat. The function $\omega_I(\underline{y})$ represents the mat thickness average distribution of velocity in the \underline{y} direction and reflects the effectiveness of flow convergence at various relative mat thicknesses. The integral of Equation (44) was evaluated numerically in a straightforward manner and $\omega_I(\underline{y})$ computed for various values of the parameters β , δ/\underline{R} , $\underline{R}/\underline{d}$. Sample graphs for $\underline{R}/\underline{d} = 0.227$, $\beta = 0$, and $\beta = 0.5$ are shown in Fig. 3 and 4, respectively. With $\omega_I = 1$ representing a local velocity equal to the approach flow velocity \underline{U} , it may be seen that, depending on the relative mat thickness, δ/\underline{R} , considerable variations of the velocity occur between the stagnation point line through $\underline{y} = 0$ and the center line between two cylinders at $\underline{y} = \underline{d}/2$, as was to be expected. By comparison, these variations are small for the mat of thickness $\delta = 6.4\underline{R}$, which indicates that a great portion of its volume would lie outside the domain of flow convergence.

In order to render Equation (44) comparable with Equation (26), a final integration is required yielding the mat space mean velocity. For reasons of symmetry, it suffices to integrate over the range $0 \leq \underline{y} \leq \underline{d}/2$, which may result in

$$\left(\frac{1}{a} \right) \frac{2}{\delta d} \int_0^{d/2} (h_o - h_1) dy = \frac{1}{a} \frac{\Delta h}{\delta} = U \bar{\omega}_I \quad (45),$$

where

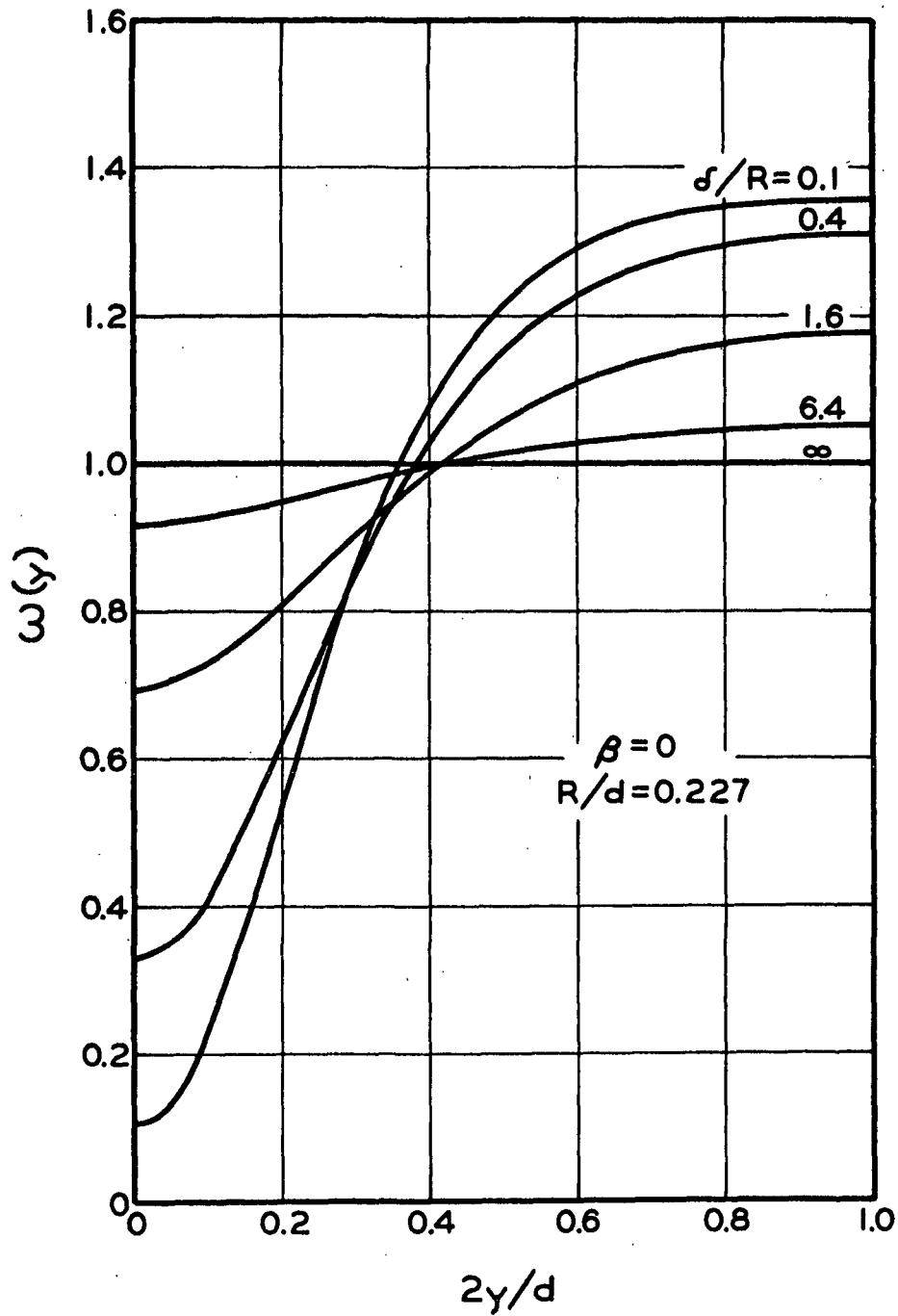


Figure 3. Mat Thickness Average Distribution $\omega(y)$ of Velocity over the Half Space Between Two Adjacent Cylinders for $\beta = 0$ (Straight Bridging Mat)

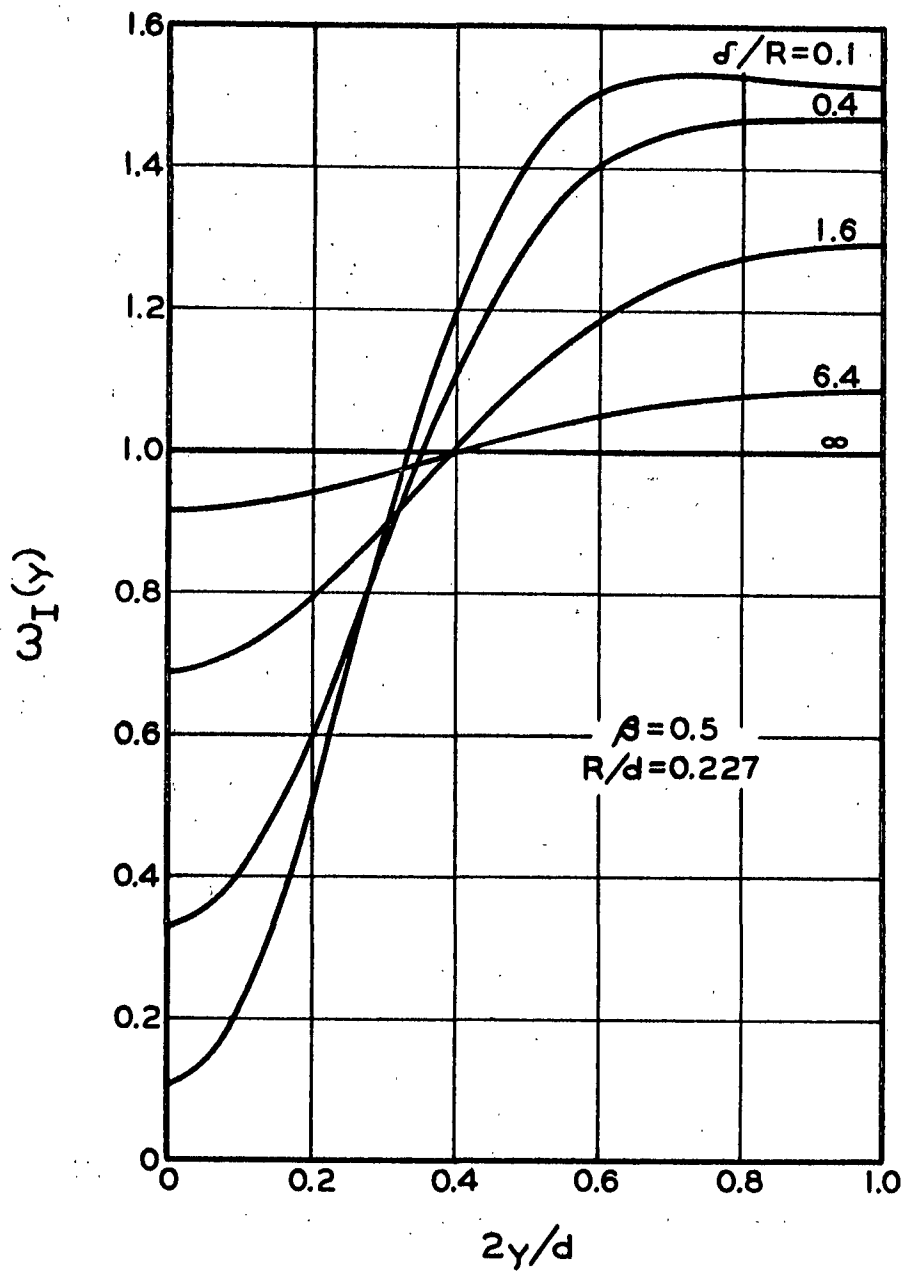


Figure 4. Mat Thickness Average Distribution $\omega_I(y)$ of Velocity over the Half Space Between Two Adjacent Cylinders for $\beta = 0.5$ (Mode I Mat)

$$\bar{\omega}_I = \frac{2}{d} \int_0^{d/2} \omega_I(y) dy = 1 - \frac{2 \sinh^2 \delta/2}{\pi X_1} \int_0^{\pi} \int_0^{X_1} F(X, Y) dXdY \quad (46),$$

and is now a function of parameters only, i.e., $\bar{\omega} = \bar{\omega}(\underline{R/d}, \beta, \delta/\underline{R})$.

A comparison of the Equations (45) and (26) leads to the following general conclusion: Provided the value of the double integral in Equation (46) does not vanish, i.e., provided $\bar{\omega} \neq 1.0$, flow convergence is effective and principally invalidates Equation (26). The application of the latter would imply an error whose magnitude depends on basis weight and/or relative thickness of the mat, δ/\underline{R} , on the relative depth of mat penetration into the wire space, β , and on the porosity of the wire, as expressed by $\underline{R/d}$. Flow convergence can be taken into account by applying a flow convergence factor, $\bar{\omega}$, to the superficial velocity, \underline{U} .

A graphical representation of $\bar{\omega}_I$ is shown in Fig. 5. The flow convergence factor decreases rapidly with increasing mat thickness, and the value $\bar{\omega} = 1$ is reached asymptotically. It increases with increasing penetration and can be very significant for very thin mats. Figure 5 also includes the case of the straight bridging mat, for which $\beta = 0$ and $\bar{\omega} = 1.0$, and which is independent of mat thickness. This somewhat surprising result may be understood by considering the various paths of integration involved.

The procedure for the case of the Mode II mat as defined above remains to be outlined briefly. The contours of the up- and downstream mat surfaces can be described by

$$x_0 = -\alpha R \quad (47)$$

and

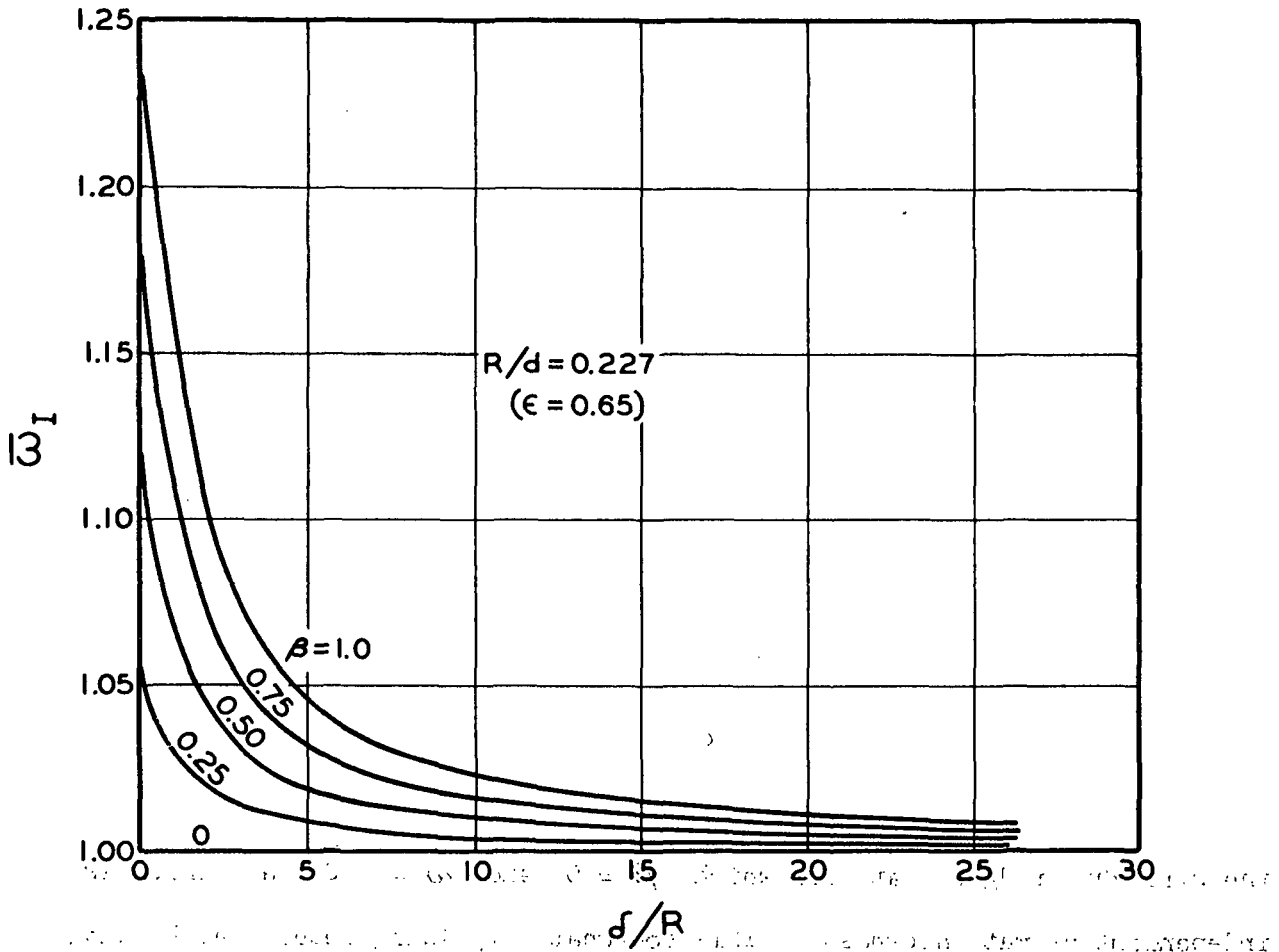


Figure 5. Flow Convergence Factor $\bar{\omega}_I$ as a Function of Penetration Factor β and Relative Mat Thickness δ/R (Mode I Mat)

$$x_1 = -R[1 - \beta \sin^2(\pi y/d)] \quad (48)$$

so that, with the auxiliary mat thickness co-ordinate ξ ,

$$x = R \{ [\alpha - 1 + \beta \sin^2(\pi y/d)] \xi - \alpha \} \quad (49)$$

and

$$\partial x = R[\alpha - 1 + \beta \sin^2(\pi y/d)] \partial \xi \quad (50)$$

Upon introduction of the independent variable Y according to definition (38) together with the above Equations (49) and (50) into Equation (27), the integration process, similar to the one outlined in detail for Mode I, yields the result:

$$\frac{1}{a} \frac{\Delta h}{\bar{\sigma}} = U \bar{\omega}_{II}$$

$$\bar{\omega}_{II} = 1 - \frac{2 \sinh^2(Y/2)}{[\alpha - 1 + (\beta/2)]} \int_0^{\pi} \{ [\alpha - 1 + \beta \sin^2(Y/2)] \int_0^1 G(\xi, Y) d\xi \} dY$$

$$G(\xi, Y) = \frac{\cosh g(\xi, Y) \cos Y - 1}{[\cosh g(\xi, Y) - \cos Y]^2}$$

$$g(\xi, Y) = \{ \gamma [\alpha - 1 + \beta \sin^2(Y/2)] \xi - \alpha \}$$
(51),

where the average mat thickness,

$$\bar{\sigma}/R = \alpha - 1 + (\beta/2) \quad (52),$$

and where γ is defined with Equation (43). The result of the numerical evaluation of the above formula for the correction factor $\bar{\omega}_{II}$ is represented graphically in Fig. 6. By comparison with Fig. 5, it may be seen that $\bar{\omega}_{II} > \bar{\omega}_I$ in the lower mat thickness range. This difference stems from the nonuniform thickness distribution of the Mode II mat, which is generally such that a comparatively greater volume portion is exposed to the higher velocities than is the case with the uniform Mode I mat.

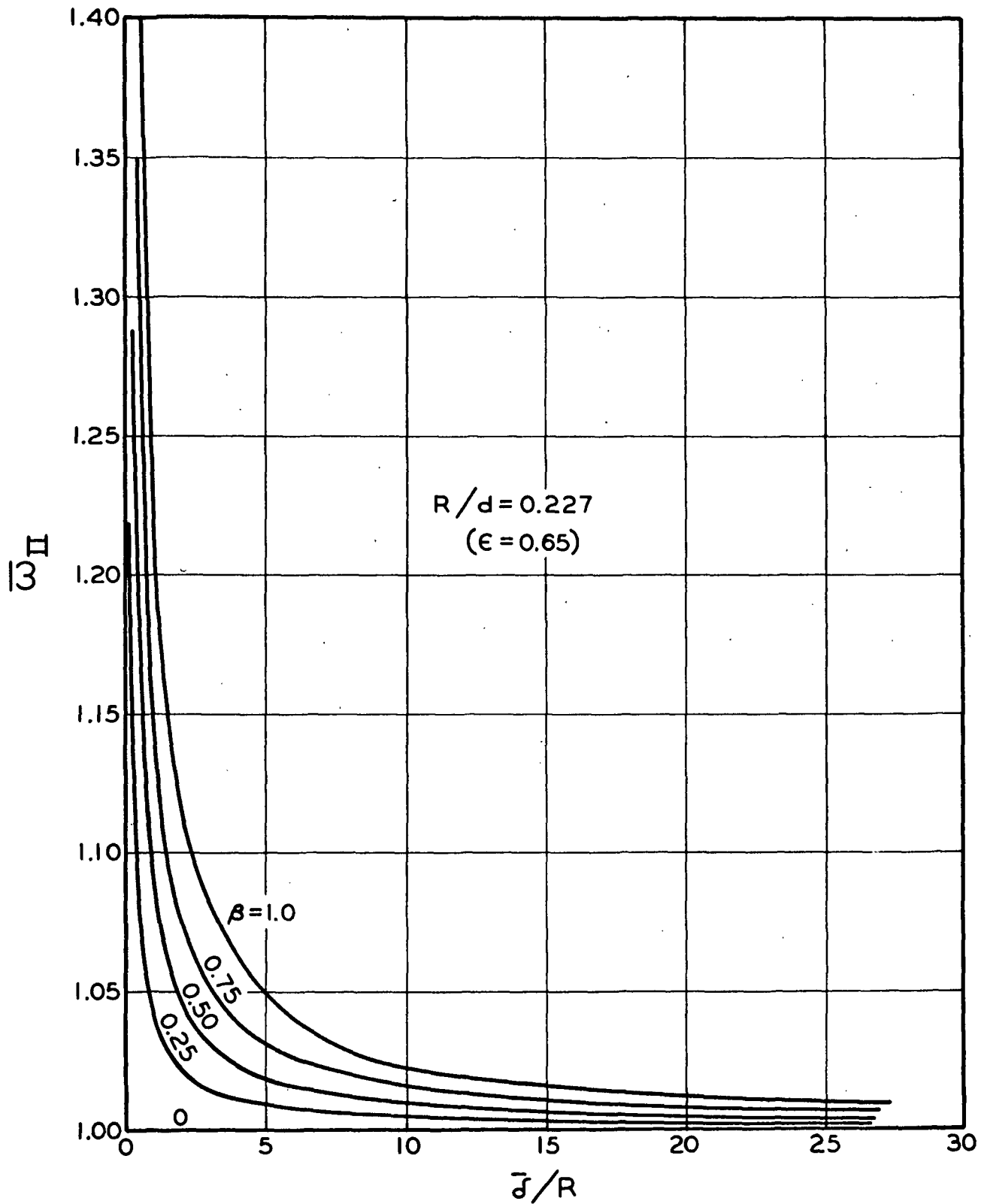


Figure 6. Flow Convergence Factor $\bar{\omega}_{II}$ as a Function of Penetration Factor β and Relative Mat Thickness $\bar{\sigma}/R$ (Mode II Mat)

APPLICATION TO EXPERIMENTS

Experiments with wood pulp fibers on ordinary wires do not fulfill the conditions under which the foregoing flow convergence formulas were derived. Nevertheless, their application appears to be justified for the following reasons. There is common agreement that a knowledge of porosity can, to a considerable degree, substitute for the exact geometric description of the porous medium. On this basis, it seems that it would not matter much that we dealt with a planar array of cylinders instead of a real wire. Further, wood pulp fibers are not incompressible and offer, therefore, a varying resistivity. Also, the superficial velocities of flow through the mats are usually beyond those of the purely viscous regime. We may, however, expect that none of these adverse conditions would cause any dramatic changes of the flow convergence factor. All in all, we assume that the flow convergence factors $\bar{\omega}_I$ or $\bar{\omega}_{II}$ are correct as to their order of magnitude.

The pressure drop-velocity data of Fig. 7 for a classified wood pulp, with $\underline{M} = 0.00215$ and $\underline{N} = 0.375$ as the familiar compressibility constants, were obtained by applying the separation Equation (3) to the raw dynamic drainage tester data. By cross plotting of the reduced data given in Fig. 12-15 (pages 53-56) in a fashion described in earlier work (2), the experimental points of Fig. 7 are obtained. Two different wire screens, 65 and 100 mesh, were used with $\underline{R} = 0.0094$ and $\underline{R} = 0.0053$ as their respective wire radii. As the data points show, there is, considering the range of experimental errors, very little difference in pressure drop for the 80-g./m.² mat; however, rather distinct ones for the 10-g./m.² mat, depending upon the type of supporting wire screen being used. We may expect that for equal velocities and thus drag forces, the penetration of deposited fibers into the wire structure will increase with decreasing number of supports per average

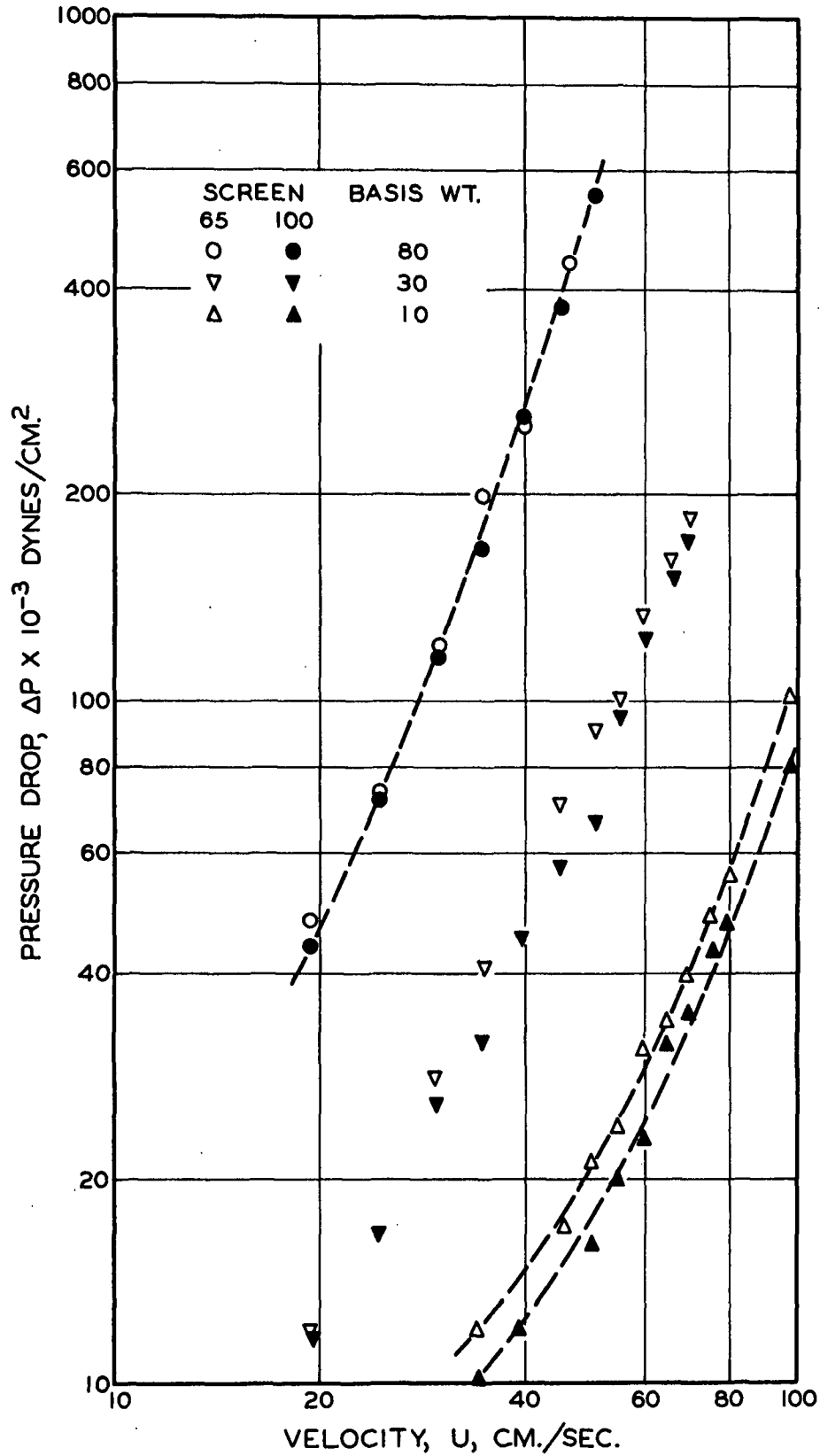


Figure 7. Pressure Drop-Velocity Data for Three Basis Weights of Wood Pulp Mats on 65 and 100-Mesh Wires (Dotted Lines = Assumed Representative Curves)

fiber length. Therefore, the penetration factor β will be larger for the 65 than for the 100-mesh wire. Considering that the relative mat thicknesses d/\underline{R} of the two mats differ by a factor of 8, it may be seen that the experiments follow the predicted trends.

A check of the predicted magnitude of the correction $\bar{\omega}$ for flow convergence depends on the quality of pressure drop predictions by use of the standard formula:

$$\left. \begin{aligned} \Delta P &= aU + bU^2, \\ a &= BW\mu k(1 - \epsilon) \bar{v}^{-3} S_V^3, \\ b &= 0.1BW\rho \sqrt{k} \bar{v}^{-3} S_V, \\ 5.5 &\leq k \leq 3.5 \epsilon^3 [1 + 57(1 - \epsilon)^3] (1 - \epsilon)^{-1/2} \quad \text{for } \epsilon \cong 0.76, \\ \epsilon &= 1 - MIV\Delta P^N \end{aligned} \right\} (53),$$

which is an integrated form (2) of Equation (2). According to standard procedure, specific volume \bar{v} and surface

$$\bar{S}_W = \bar{v} \bar{S}_V \quad (54)$$

are obtained as mean values by evaluating constant-rate filtrations as repeatedly described in earlier work by means of the viscous flow correlation (2)

$$\left. \begin{aligned} \frac{\Delta P}{c^{1/2} t} &= m_1 + m_2 c^3, \\ m_1 &= 3.5 [1 - (N/2)] \mu \rho S U^2 \bar{v}^{3/2} \bar{S}_V^2, \\ m_2 &= 57 [1 - (N/2)]^6 \bar{v}^3, \quad \text{and} \end{aligned} \right\} (55)$$

$$c = \text{MAP}^N \quad (55a).$$

A plot according to this relationship for the pulp used in the experiments of Fig. 7 is shown in Fig. 8. The familiar straight-line technique (not shown) yields the values

$$\bar{v} = 2.35 \text{ cm.}^3\text{g.}^{-1} ; \quad \bar{S} = 5350 \text{ cm.}^2\text{g.}^{-1}$$

for use in Equation (53). The relative mat thickness may be found from

$$d/R = \text{BW}/R[1 - (N/2)]^2 \text{MAP}^N \quad (56),$$

yielding for the 80-g./m.² mat and a range average pressure drop of $\Delta P = 10^3$ dynes/cm.²

$$d/R = 8.0 \quad \text{and} \quad 14.2$$

for the 65 and 100-mesh wires, respectively. For the rather long fibers of the experiments, the Mode I model of mat cross section appears to be the more realistic one, and Fig. 5 gives

$$\bar{\omega}_I \leq 1.028 \quad \text{and} \quad \leq 1.017$$

as correction factors for the above two cases. These values are well within the limits of experimental error, and Equation (53) would apply, with good approximation as it stands, to the 80-g./m.² mat.

With the pulp used in Ingmanson and Andrews' previous experiments (2), it was possible to fit the prediction according to Equation (53) to the data by varying the integration constant \underline{I} of the accompanying porosity formula as a function of basis weight. This method was again applied, and by use of the values of \bar{v} , \bar{S} , \underline{M} , and \underline{N} , as mentioned in the text, the solid-line curves in Fig. 9

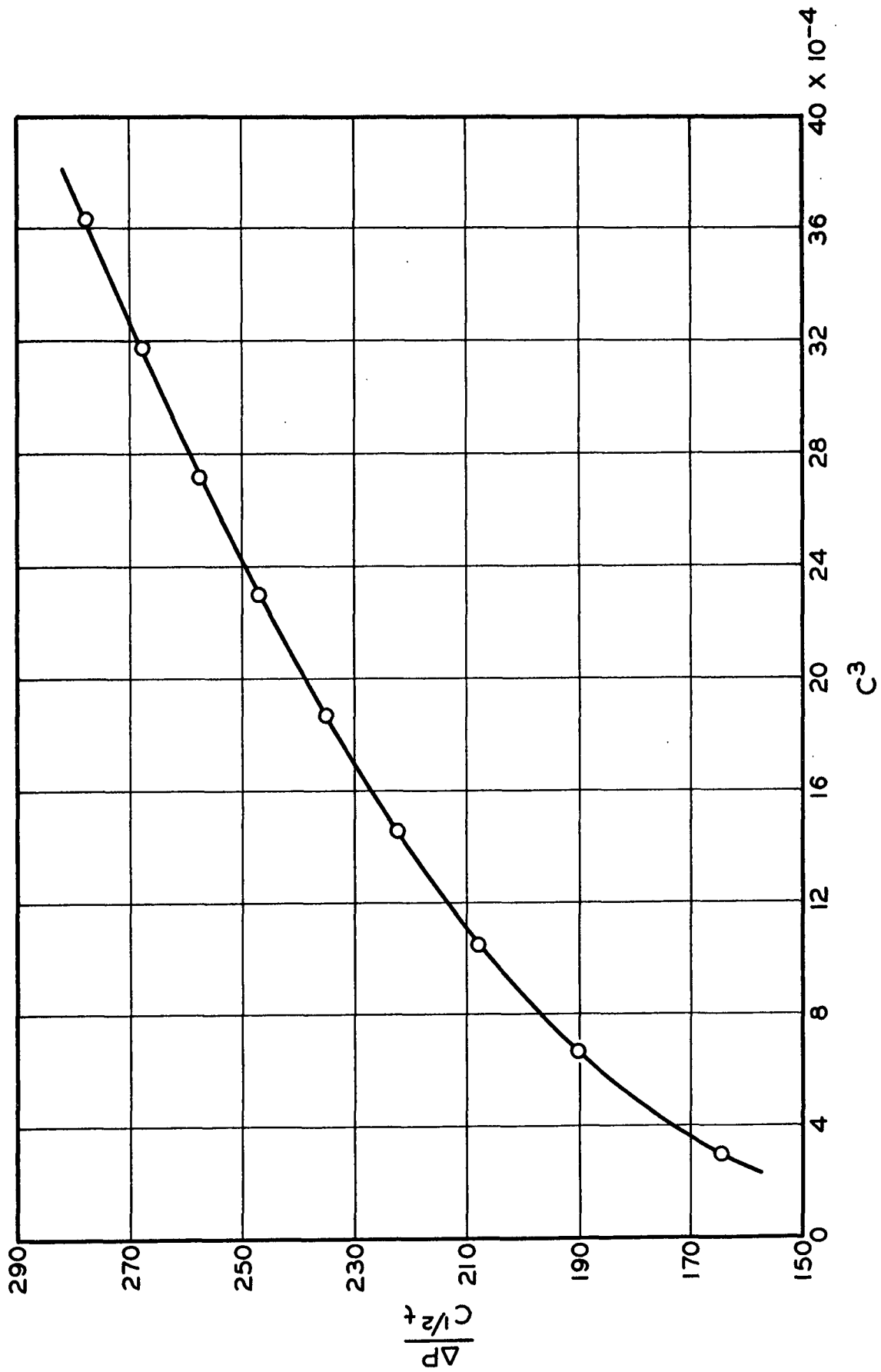


Figure 8. Rectified Plot of Data for Viscous Flow Filtration

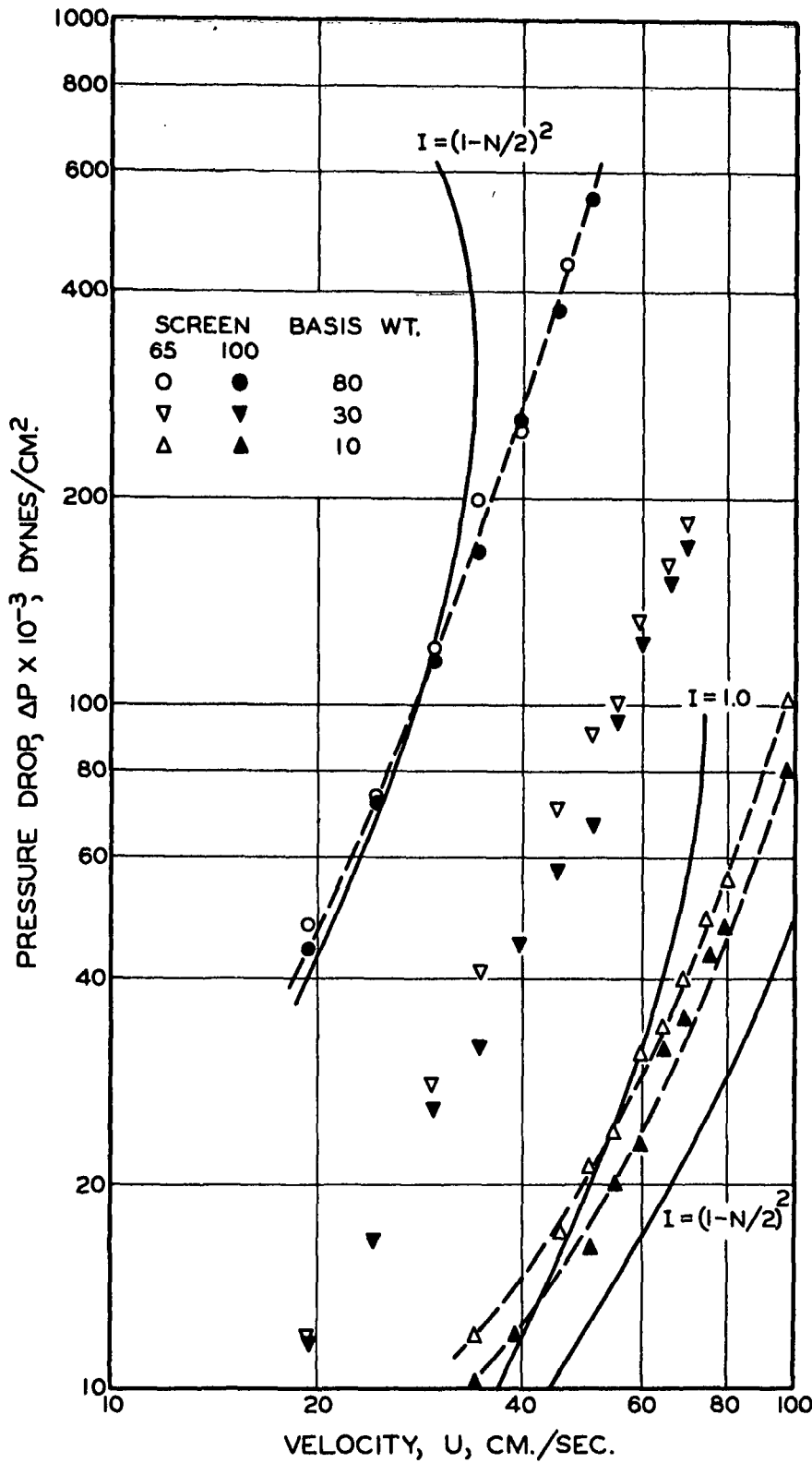


Figure 9. Comparison of Data and Their Prediction by Equation (53)
(Constant Specific Volume \bar{v} and Surface \bar{S}_w
Variation of Integration Factor I)

were obtained for mats of basis weights 80 and 10 g./m.² Evidently, variations of \underline{I} within the limits $[1 - (\underline{N}/2)]^2 \leq \underline{I} \leq 1.0$ would have failed to produce the same favorable fit as the one previously reported and was therefore not attempted.

The compressibility constants \underline{M} and \underline{N} as well as specific volume and surface \bar{v} and \bar{S} , respectively, are, according to standard procedure, procured from evaluation of thick mat experiments. Thus, in unsuccessfully applying known concepts to thin mats, doubts may arise as to the reliability of these values in thin mat work. Concern about the compressibility behavior of thin mats as compared with thick mats is indicated, but experimental evidence is at the present time too limited to draw final conclusions. As to fiber specific volume and surface in general, it appears that a different interpretation of basic data is possible.

In connection with experimental evidence already secured, one has reason to question the standard procedure of substituting a straight line for the constant-rate curve of Fig. 8. The evidence that a plot according to Equation (55) does not yield a straight line points to the fact that specific volume and surface vary. An approximate method of obtaining varying \bar{v} and \bar{S} may be outlined as follows. For the sake of abbreviation, write Equation (55) in the form

$$\begin{aligned} Y &= m_1 + m_1 m_2 X \\ m_1 &= m_{01} \bar{S}_w^2 / \bar{v}^{1/2} \\ m_2 &= m_{02} \bar{v}^3 \end{aligned} \quad \left. \vphantom{\begin{aligned} Y &= m_1 + m_1 m_2 X \\ m_1 &= m_{01} \bar{S}_w^2 / \bar{v}^{1/2} \\ m_2 &= m_{02} \bar{v}^3 \end{aligned}} \right\} (57).$$

Assume two very close points, $\underline{X}_{\mu-1}$, $\underline{Y}_{\mu-1}$ and \underline{X}_{μ} , \underline{Y}_{μ} , anywhere along the curve of Fig. 8 and assume that \bar{v} and \bar{S}_w are representative mean values.

$$\bar{v} = \frac{1}{\Delta P_{\mu} - \Delta P_0} \int_{\Delta P_0}^{\Delta P_{\mu}} v d(\Delta P) \quad (58)$$

and similarly for \bar{S}_W . Then Equation (57) yields

$$\bar{v} = \left[\frac{Y_{\mu} - Y_{\mu-1}}{(X_{\mu} Y_{\mu-1} - X_{\mu-1} Y_{\mu}) m_{O_2}} \right]^{1/3} \quad (59)$$

$$\bar{S}_W = \left[\frac{X_{\mu} Y_{\mu-1} - X_{\mu-1} Y_{\mu}}{m_{O_1} (X_{\mu} - X_{\mu-1})} \right]^{1/2} \bar{v}^{1/4} \quad (60)$$

The point pressures in Equation (59) can be obtained from the compressibility equation, i.e. from

$$\Delta P_{\mu} = \left(\frac{X_{\mu}^{1/3}}{M} \right)^{1/N} \quad (61)$$

In order to avoid losing accuracy by reading point values from the graph of Fig. 7, Lagrange's interpolation formula,

$$\left. \begin{aligned} Y_{\mu} &= \sum_{i=1}^9 \frac{\Pi_9(X_{\mu})}{(X_{\mu} - X_i) \Pi_9'(X_{\mu})} Y_i \\ \Pi_9(X_{\mu}) &= (X_{\mu} - X_1)(X_{\mu} - X_2) \dots (X_{\mu} - X_9) \\ \Pi_9'(X_{\mu}) &= \frac{d}{dX_{\mu}} \Pi_9(X_{\mu}) \end{aligned} \right\} \quad (62)$$

was used, where the X_i , Y_i , $i = 1, 2, \dots, 9$ are the nine experimental points of Fig. 8. The point results of this evaluation are shown in Fig. 10 along Curves (a), (b), and (c), representing \bar{v} , \bar{S}_V , and \bar{S}_W as functions of pressure drop, ΔP .

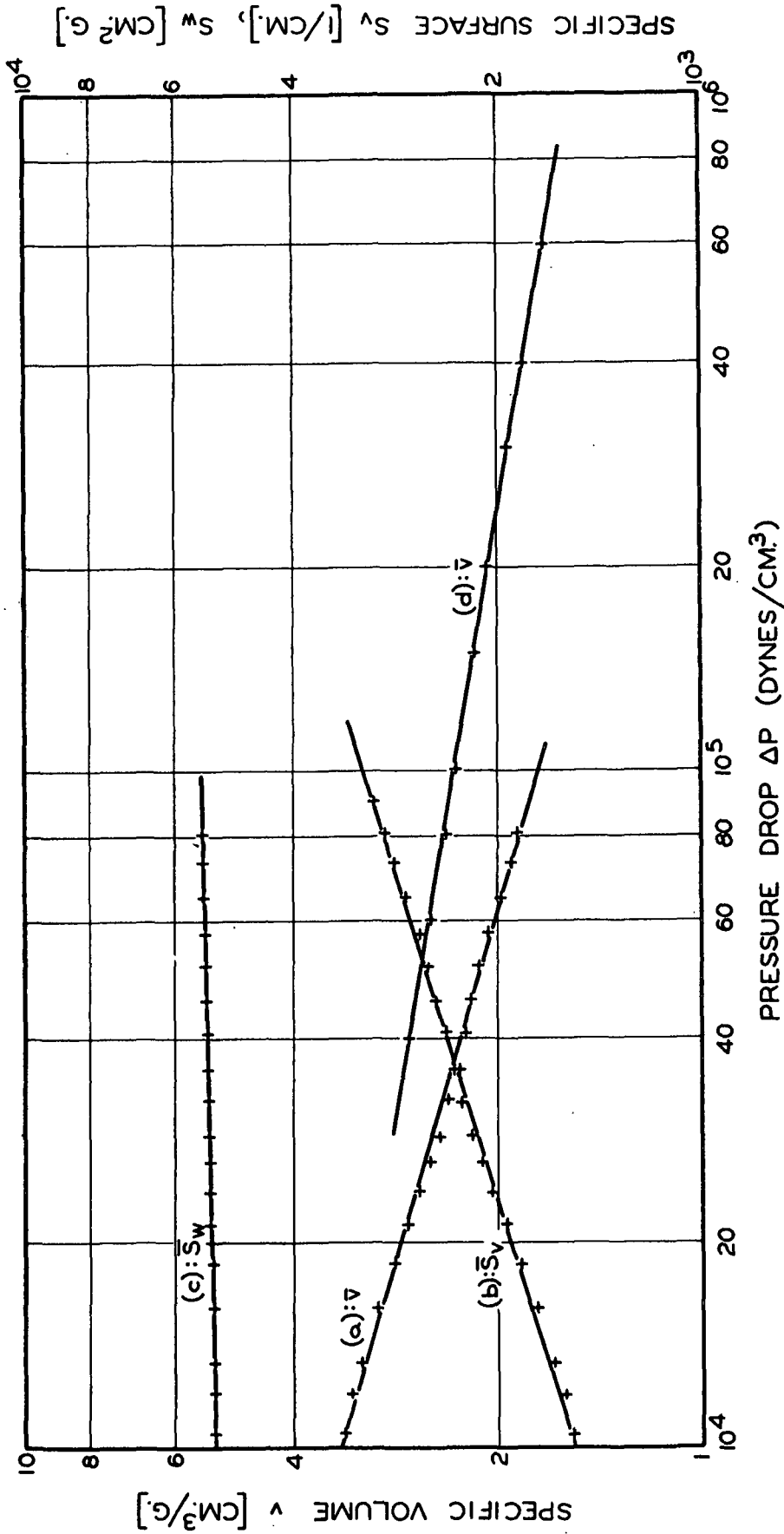


Figure 10. Specific Volume \bar{v} and Surfaces \bar{S}_v and \bar{S}_v as Obtained from Filtration and Dynamic Drainage Runs. Curves (a), (b), (c) from Filtration Experiment; Curve (d) from 80-g./m.² Mat Drainage Tester Run. (+ = Computed Points; - = Arbitrarily Drawn Curves.)

As may be seen, the above-mentioned average values, \bar{v} and \bar{S}_w , as obtained by the straight-line method fall within the range of total variation resulting from the new method. Specific volume \bar{v} decreases while specific surface \bar{S}_w increases with increasing pressure drop. Both variations are in accordance with physical expectation and simply mean that applied stresses reduce the amount of water a pulp fiber is capable of imbibing by swelling. There is also evidence that specific surface on a weight basis, i.e. \bar{S}_w , should change only very little, if at all. It can be seen that \bar{S}_w may be represented in the form

$$\bar{S}_w \approx 4450 \Delta P^{0.0177} \quad (63).$$

Evidently, the increase in interfiber contact area (2) which would make \bar{S}_w decrease with increasing pressure is more than counterbalanced by a substantial gain in flow-exposed surface due to flattening of the wood fibers. Assuming that the numerical values of \bar{S}_w thus available would be typical of the pulp used rather than the type of experiment, this function was introduced into Equation (53), the coefficients of which may, in terms of \bar{S}_w , be written as

$$\left. \begin{aligned} a &= BWLM[1 - (N/2)]^2 \Delta P^N k e^{-3\bar{S}_w^2} \\ b &= 0.1BW\rho \sqrt{k} e^{-3\bar{S}_w} \\ c &= 1 - M[1 - (N/2)]^2 \bar{v} \Delta P^N \end{aligned} \right\} \quad (86a, b, c)$$

and applied to the 80-g./m.² mat data as represented by the dotted line of Fig. 7 to evaluate for specific volume. The necessary computations are purely algebraic involving the repeated numerical solution of a transcendental equation and need not be demonstrated here. The result may be found as Curve (d) in Fig. 10 for comparison with Curve (a) as obtained from the constant-rate filtration run. In a log-log plot, the computed points constitute points along a straight line, yielding

$$\bar{v} \approx 16.62P^{-0.1723} \quad (65)$$

as a very good representation of Curve (d).

In discussing the two considerably different results for the same pulp, we may temporarily disregard the fact that both Curves (a) and (d) represent mat average values according to Equation (58). Constant-rate filtration experiments are conducted in the viscous range of flow, and the time lapse at the first and the last point of Curve (a) was 200 and 800 seconds of forming time, respectively. In contrast, to form an 80-g./m.² mat on the dynamic drainage tester requires only between 1 and 3 seconds. The results from both experiments depend, of course, on the compression response of the fibrous networks, i.e., on the compressibility constants \underline{M} and \underline{N} . However, it was shown for thick mats (7) that the times involved in both experiments are far beyond the ones where creep is effective. There remain, then, two other possibilities which could account for the difference.

1. The above-mentioned compressibility constants, $\underline{M} = 0.00215$ and $\underline{N} = 0.375$, were obtained under stationary environmental conditions, i.e., in the absence of any vibrations. There exists preliminary experimental evidence that vibrations cause the mats to become semimechanically conditioned if vibrations are present, resulting primarily in increased \underline{M} values.

2. In thin mats, the number of fiber-to-fiber contacts per fiber which actively participate in deforming the fiber cross sections may be smaller than in thick mats. No mathematical proof of this assumption has been attempted so far. If it should hold, it implies the further assumption that fiber longitudinal stresses resulting from flow drag would contribute only insignificantly to deformation of the fiber cross section.

Both filtration and compressibility experiments are usually executed in the absence of disturbances. For this reason, it may be assumed that within the limitations of Equation (55) with regard to the Kozeny factor, k , itself (influence of cross-sectional shape!) the \bar{v} values according to Curve (a) in Fig. 10 are representative of this type of experimental condition.

The rack gear to the piston of the dynamic drainage tester introduces considerable oscillations to flow and apparatus [see Fig. 25 in (2)] which would tend to mechanically condition the thin mats being formed. According to the above-mentioned preliminary findings, it would consequently be necessary to apply a higher M value in this case. It could be shown that such a measure would indeed displace Curve (d) toward Curve (a) and approximately parallel to itself.* One would, however, still have to resort to the above second argument in order to account for the remaining discrepancy between the two slopes.

Specific volume according to Equation (65) as obtained by evaluating the 80-g./m.² run of Fig. 7 is, of course, the result of curve fitting. Fortunately, its relationship with regard to applied pressure drop is also physically reasonable, and our findings may therefore be used to predict the pressure drops for the 30 and 10-g./m.² mats. We might consider proceeding from the original Equation (2) instead of from its integral form (53), which would require a knowledge of point values v and $\frac{S}{W}$ instead of the mean values \bar{v} and $\bar{\frac{S}{W}}$ as available from Equations (65) and (63). Writing the Equations (65) and (58) in their general form,

* It may be mentioned that the set of equations

$$\begin{aligned}\Delta P &= \Delta P(U) \quad (\text{experimental points}) \\ \Delta P &= a(\Delta P, \bar{v})U + b(\Delta P, \bar{v})U^2 \quad (53) \text{ with } (64a, b, c)\end{aligned}$$

does not have roots \bar{v} for any set of M and N values. In particular, there is no real (i.e., physically meaningful) solution for the set $M = 0.0339$; $N = 0.158$, which may be considered as being typical for a fully mechanically conditioned wood pulp mat [values obtained from (2), Fig. 10].

$$\bar{v} = M_V \Delta P^{-N_V} \frac{1}{\Delta P - \Delta P_0} \int_{\Delta P_0}^{\Delta P} v d(\Delta P) \quad (66),$$

where ΔP_0 may be the pressure drop across the mat top fiber layer, one easily obtains

$$v = M_V \Delta P^{-N_V} \{1 - N_V [1 - (\Delta P_0 / \Delta P)]\} \quad (67)$$

as the corresponding point specific volume. For very thick mats, obviously, $\Delta P_0 / \Delta P \ll 1$, and $\Delta P_0 / \Delta P = 1$ for a very thin mat one fiber diameter thick. An analogous relationship would have resulted for $\frac{S}{W}$. It may be noted in passing that ΔP_0 would depend on both superficial velocity and porosity of the top layer. Use of Equation (67) and arriving at an integrated flow equation would be rather cumbersome. It was therefore preferred to apply Equations (53) and (64a, b, c) with \bar{v} and $\frac{S}{W}$ as given by the Equations (63) and (65). The results for the 30 and 10-g./m.² mats are plotted as solid lines and compared with the experimental points in Fig. 11.

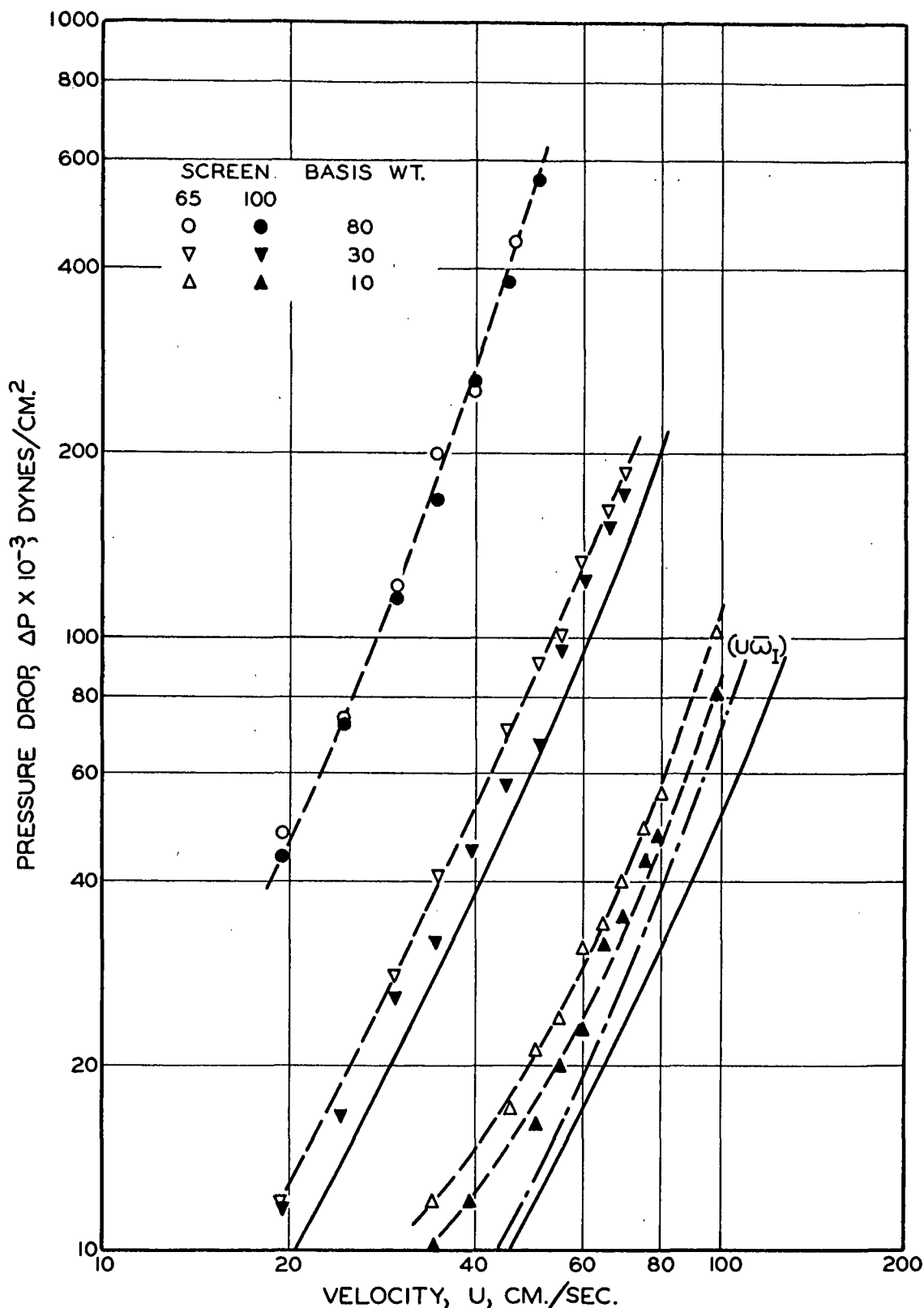


Figure 11. Comparison of Experiments with Predictions as Resulting from Varying Specific Volume and Surface. Experimental Points and Predicted Solid Curves. (--- Corrected for Flow Convergence According to $\bar{\omega}_I$.)

DISCUSSION OF RESULTS AND CONCLUSIONS

It will be noted from Fig. 11 that the predicted pressure drops for the 30 and 10-g./m.² mats fall increasingly short of the experimental points with decreasing basis weight, thus generally confirming the predicted effect of basis weight or mat thickness ratio, d/R , on flow convergence. The correction factor $\bar{\omega}$, however, which would have to be applied in order to make the predicted pressure drops coincide with the experimental points, is considerably higher than those obtainable from either one of the graphs, Fig. 5 or Fig. 6, when the proper mat thickness ratios, d/R , are taken for the respective mats and wires. In Fig. 11 the dotted curve labeled $(\underline{U}\bar{\omega}_I)$ represents the prediction corrected for the effect of flow convergence by use of the graph of Fig. 5. Although a number of grave assumptions and simplifications had to be made in order to arrive at the reported theoretical flow convergence factors $\bar{\omega}_I$ and $\bar{\omega}_{II}$, it is felt that a final verdict regarding the compatibility of these values as well as that of the separation Equation (3) should be postponed pending further experimental clarification in connection with the parameters \underline{M} , \underline{N} , \underline{v} , and \underline{S}_w for thin wood pulp mats. Such a decision recommends itself in view of Ingmanson and Andrews' results for thin mats of synthetic fibers (1). Bearing in mind that their thin mats on 28-mesh wires suffered, due to only partial fiber retention from a pronounced lack of randomness, their results for the 100-mesh wire [see their Fig. 10 (1)] indicates that with fiber specific volume and surface reliably known, predictions and experimental points come close enough for successfully applying the predicted corrections. Regarding thin mats from wood pulp fibers, clarification of the following points of interest is suggested.

1. As preliminary tests seemed to indicate, the result of compressibility experiments (i.e., factor \underline{M} and exponent \underline{N}) might depend on the degree of

vibrational shake of apparatus and mat. This should be confirmed under well-defined conditions. For the sake of simplification and in view of the difficulty involved in simulating the same condition during compressibility experiments, however, the rack-and-pinion piston gear to the dynamic drainage tester must be replaced by a continuous drive.

2. It should be established whether or not there is a dependence of \underline{M} and \underline{N} on the basis weight of the mat under compression.

3. There appears to be little doubt left that fiber specific volume \underline{v} decreases with increasing mat compression, i.e., with increasing applied stress. With the time effect on compression response between filtration and dynamic drainage test ruled out, a very significant conditional difference between the two experiments is the respective basis weights. In comparing the two curves, (a) and (d) of Fig. 10, for specific volume, one might tentatively conclude that for the same area-related stress an average individual fiber in a very thick mat would suffer a higher reduction of specific volume than one in a very thin mat. Notice that Curve (a) was arbitrarily drawn and that most computed points fall short in a rather systematic way. This could be due to the continuously increasing basis weight.

4. It appeared to be somewhat unsatisfactory that in evaluating the 80-g./m.² mat, flow data for fiber specific volume, \underline{v} , and specific surface, \underline{S}_w , as previously obtained from the filtration experiment had to be taken. In an attempt to calculate both \underline{v} and \underline{S}_w from the same experimental data by separating viscous and inertial contributions to the total mat pressure drop, it was rigorously proved that this is impossible. (See Appendix.)

5. The eventual dependence of fiber specific volume on a basis weight-dependent parameter could be established by the evaluation of experimental data for mixed flow through mats of basis weights between 100 and 300 g./m.² In view of the findings of this report, the dependence of specific volume on pressure drop should show decreasing slope with increasing basis weight.

6. In the above attempts to improve pressure drop predictions for thin mats, it was quickly realized that thin mats evidently conform to the wire structure as well as changing their structural density with increasing stress. The latter observation is in contrast to the assumption of constant mat resistivity applied in connection with the solution of Equation (14). It would be desirable to solve Equation (14) by a series expansion of the solution (21) whereby a reasonably simple expression for the resistivity $\underline{a}(\underline{x}, \underline{y})$ could be employed.

7. The problem underlying the separation Equation (3) cannot be solved satisfactorily by way of theory only. Independent experiments must be designed which take advantage of model laws applied to rigid but similar structures which can be separated and measured separately.

NOMENCLATURE

\underline{A}	=	fiber mat area projected in flow direction, cm. ²
$\frac{\underline{a}}{\underline{a}_0}, \frac{\underline{b}}{\underline{b}_0}$	=	viscous and inertial resistivity of fiber mat, c.g.s. units
\underline{C}_ν	=	ν -th coefficient in series of Equation (79)
\underline{c}	=	local mat consistency, g./cc.
\underline{d}	=	pitch of cylinder array, cm.
$F()$	=	function of ()
$f()$	=	function of ()
$G()$	=	function of ()
$g()$	=	function of ()
\underline{h}	=	piezometric head, c.g.s. units
$\Delta \underline{h}$	=	head loss, c.g.s. units
\underline{I}	=	porosity distribution factor, dimensionless
\underline{k}	=	Kozeny factor, dimensionless
$\underline{M}, \underline{N}$	=	compressibility constants, c.g.s. units and dimensionless
$\frac{\underline{M}}{\underline{V}}, \frac{\underline{N}}{\underline{V}}$	=	coefficient and exponent of power law representation of fiber specific volume, c.g.s. units and dimensionless, respectively
$\underline{m}_1, \underline{m}_2$	=	coefficients in rectified filtration equation, c.g.s. units
$\Delta \underline{P}$	=	pressure drop across the fiber mat, c.g.s. units
\underline{p}	=	local pressure inside mat, c.g.s. units
\underline{R}	=	radius of shute or warp wire, cm.
\underline{Re}	=	Reynolds number
$\frac{\underline{S}}{\underline{V}}, \frac{\underline{S}}{\underline{W}}$	=	fiber specific surface on a volume and weight basis, respectively, cm. ⁻¹ and cm. ² /g., respectively
\underline{t}	=	time, sec.
\underline{U}	=	superficial velocity of main flow through fiber mat
$\underline{u}, \underline{v}, \underline{w}$	=	components of superficial velocity in three-dimensional flow, cm./sec.

- \underline{v} = fiber specific volume, cc./g.
- \underline{W} = mass of fibers in a mat, g.
- $\underline{W}/\underline{A}$ = basis weight of fiber mat, g./cm.²
- $\underline{X}, \underline{Y}$ = introduced for purposes of abbreviation and defined in text
- $\underline{x}, \underline{y}, \underline{z}$ = Cartesian co-ordinate system
- $\underline{x}, \underline{y}$ = introduced for purposes of abbreviation and defined in text
- α = dimensionless mat thickness
- β = mat penetration factor, dimensionless
- γ = defined by Equation (43), dimensionless
- δ = over-all mat thickness, cm.
- ϵ = porosity, dimensionless
- ζ = vorticity at a point $\underline{x}, \underline{y}$, sec.⁻¹
- η = independent variable defined by Equation (76), dimensionless
- θ = angle between surface normal and \underline{x} axis
- μ = viscosity, poises; defined subscript, dimensionless
- ν = defined subscript, dimensionless
- ξ = auxiliary mat thickness co-ordinate, dimensionless
- Π = product function defined by Equation (62)
- ρ = density, g./cc.
- ϕ = potential function
- ψ = stream function
- $\Omega(\eta)$ = defined by Equations (76) and (79)
- $\omega(\underline{y}), \bar{\omega}$ = flow convergence factors, dimensionless

ACKNOWLEDGMENT

The author wishes to express his appreciation of numerous discussions with W. L. Ingmanson, and with B. D. Andrews who also provided the experimental data used in this report.

LITERATURE CITED

1. Ingmanson, W. L., and Andrews, B. D. Studies of the sheet-forming process - Permeation of thin fiber mats. Progress Report Two, Project 2348. Appleton, Wis., The Institute of Paper Chemistry, March 29, 1963.
2. Ingmanson, W. L., and Andrews, B. D. Studies of the sheet-forming process Forming thin mats of wood fibers at high rates. Progress Report Four, Project 2348. Appleton, Wis., The Institute of Paper Chemistry, Feb. 27, 1964.
3. Flachsbart, O., Physik. Z. 28, no. 13:461(1927).
4. Rouse, H. Advanced mechanics of fluids. New York, John Wiley & Sons, Inc., 1959.
5. ~~Katschin, N. J., Kibel, I. A., and Rose, N. W. Theoretische Hydromechanik I. Berlin, Akademie-Verlag, 1954.~~
6. Ingmanson, W. L., Han, S. T., Wilder, H. D., and Myers, W. T., Jr., Tappi 44, no. 1:47-54(1961).
7. Wilder, H. D. The compression creep properties of wet pulp mats. Doctoral Dissertation. Appleton, Wis., The Institute of Paper Chemistry, 1960; Tappi 43, no. 8:715(1960).

THE INSTITUTE OF PAPER CHEMISTRY
Engineering and Technology Section

H. Meyer

H. Meyer

APPENDIX I

ON THE NUMERICAL SEPARABILITY OF VISCOUS AND INERTIAL TERMS OF THE FORCHHEIMER EQUATION BY MEANS OF ONE SET OF EXPERIMENTAL DATA

For the sake of greater convenience, Equation (53) with (64a, b, c) may be written in the form

$$F(x, y) = f(y)x + g(y)x^2 - y = 0 \quad (68).$$

Assume that it would be possible to separate for f and g at every point $\underline{x}, \underline{y}$ along an experimentally given curve $\underline{y} = \underline{y}(\underline{x})$; then we would be able to evaluate

$$\epsilon = \left[\frac{0.01 \rho^2 BW}{[1 - (N/2)]^2 M_{\mu y}^N} \cdot \frac{f}{g^2} \right]^{1/3} \quad (69)$$

with respect to specific volume, \bar{v} , by means of

$$\bar{v} = \frac{1 - \epsilon}{[1 - (N/2)]^2 M_y^N} \quad (70),$$

while specific surface, \bar{S}_w , follows from

$$\bar{S}_w = \frac{\epsilon^3}{0.1 BW \rho k^{1/2}} \quad (71).$$

Equations (69) through (71) follow from the definitions of f and g , respectively. As indicated, Equation (68) is an implicit equation with respect to \underline{y} . It is then assumed that Equation (68) is an implicit form of the explicitly given experimental data $\underline{y} = \underline{y}(\underline{x})$. By partial differentiation of Equation (68), according to elementary rules, one finds

$$\frac{\partial F}{\partial x} + \frac{dy}{dx} \frac{\partial F}{\partial y} = 0 \quad (72),$$

$$\frac{\partial F}{\partial x} = f + 2gx \quad (73),$$

$$\frac{\partial F}{\partial y} = f'x + g'x^2 - 1 \quad (74).$$

Primes mean differentiation with respect to y . Thus, a solution to Equation (72) would provide two equations, (73) and (74), for f and g . In a step-by-step procedure, it is always possible to approximate the given data by an expression like

$$y = ax^n; \quad x \sim x_0; \quad y \sim y_0 \quad (75),$$

with constant a and n , which in general might change when going to a consecutive point x_1, y_1 . Thus,

$$\frac{dy}{dx} = nax^{n-1} \quad (75a),$$

and Equation (72) may be found to have

$$F(x, y) = \Omega(\eta); \quad \eta = y - ax^n \quad (76)$$

as a general solution, so that

$$\frac{\partial F}{\partial x} = -nax^{n-1} \Omega'(\eta) \quad (77);$$

$$\frac{\partial F}{\partial y} = \Omega'(\eta) \quad (78).$$

A suitable special solution would be

$$\Omega(\eta) = \sum_{\nu=1}^{\infty} c_{\nu} \eta^{\nu} \quad (79)$$

so that for $\eta \sim 0$, approximately,

$$\Omega(\eta) \approx C_1 \eta \quad (80)$$

Equations (73) and (74) become

$$f + 2gx = -C_1 nax^{n-1} \quad (73a)$$

$$f'x + g'x^2 = 1 + C_1 \quad (74a)$$

where now the variable x may be expressed in terms of y by use of Equation (75),
whence

$$x = (y/a)^{1/n} \quad (75a)$$

A differential equation for g is obtained of the form

$$g' + \frac{2}{ny} g + a^{2/n} (1 + nC_1) = 0 \quad (81)$$

having

$$g = -a(1 + nC_1)(y/a)^{(n-2)/n} \quad (82)$$

as a solution, and f becomes

$$f = a(2 + nC_1)(y/a)^{(n-1)/n} \quad (83)$$

Upon introduction of f and g into the original Equation (68), an identity

$$1 \equiv 1 + nC_1 - nC_1 \quad (84)$$

is obtained which is satisfied for any value of C_1 . However, in order to have f and g both positive and nonzero, it must be

$$C_1 = -\frac{\alpha}{n}; \quad 1 < \alpha < 2 \quad (85).$$

This is proof that it is impossible to separate the viscous and inertial term of the Forchheimer equation (68) by means of given experimental data and equation manipulation only. Rather, an independent second set of equations and experimental data would be necessary. Practically speaking, it is a necessary and sufficient condition to know $\frac{\bar{S}}{W}$ of Equation (71).

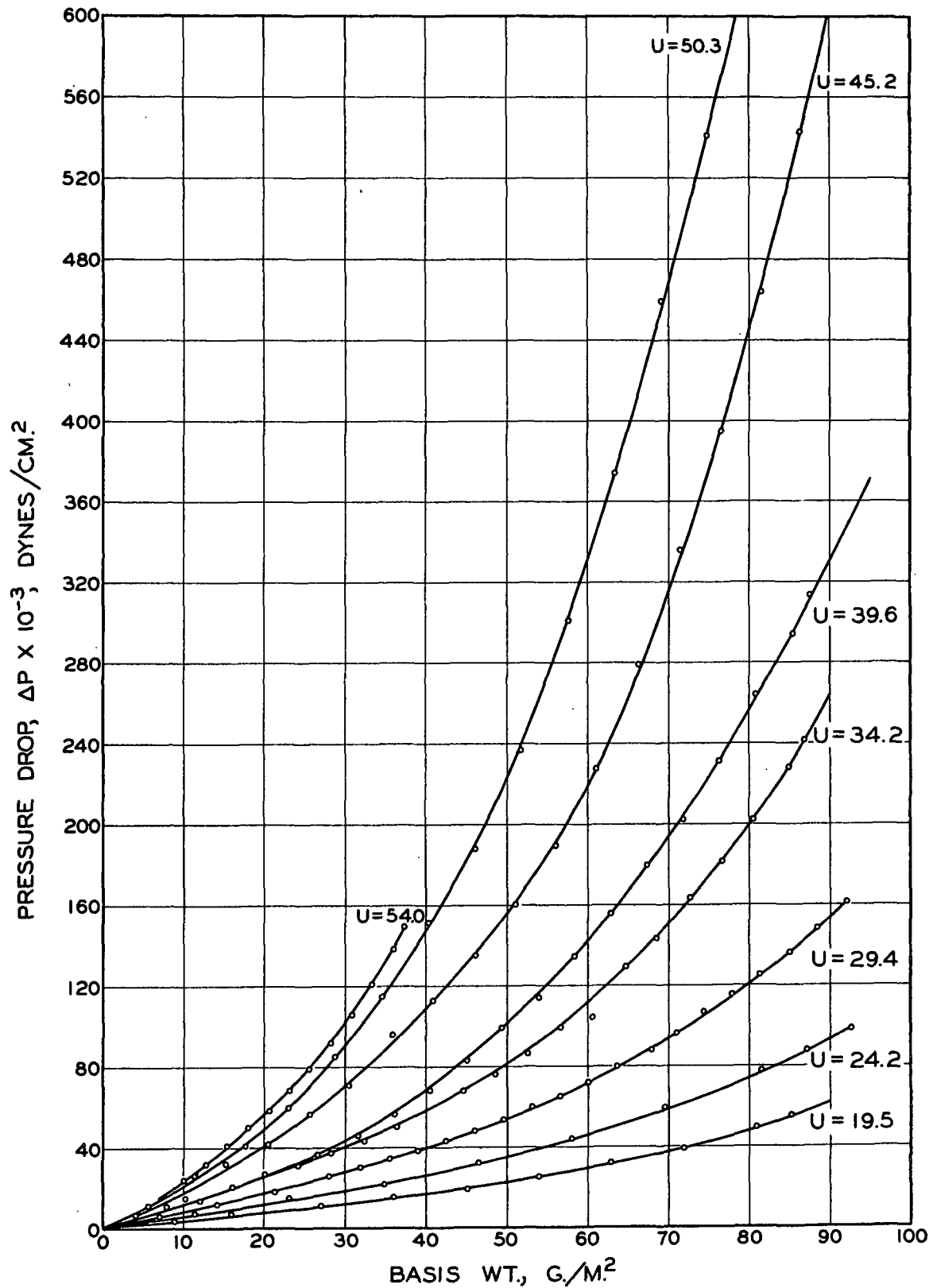


Figure 12. Dynamic Drainage Tester Run Data of Wood Pulp. Mat Pressure Drop, ΔP , as a Function of Superficial Velocity, U , and Basis Weight (Mats on 65-Mesh Wire; Lower Velocity Range)

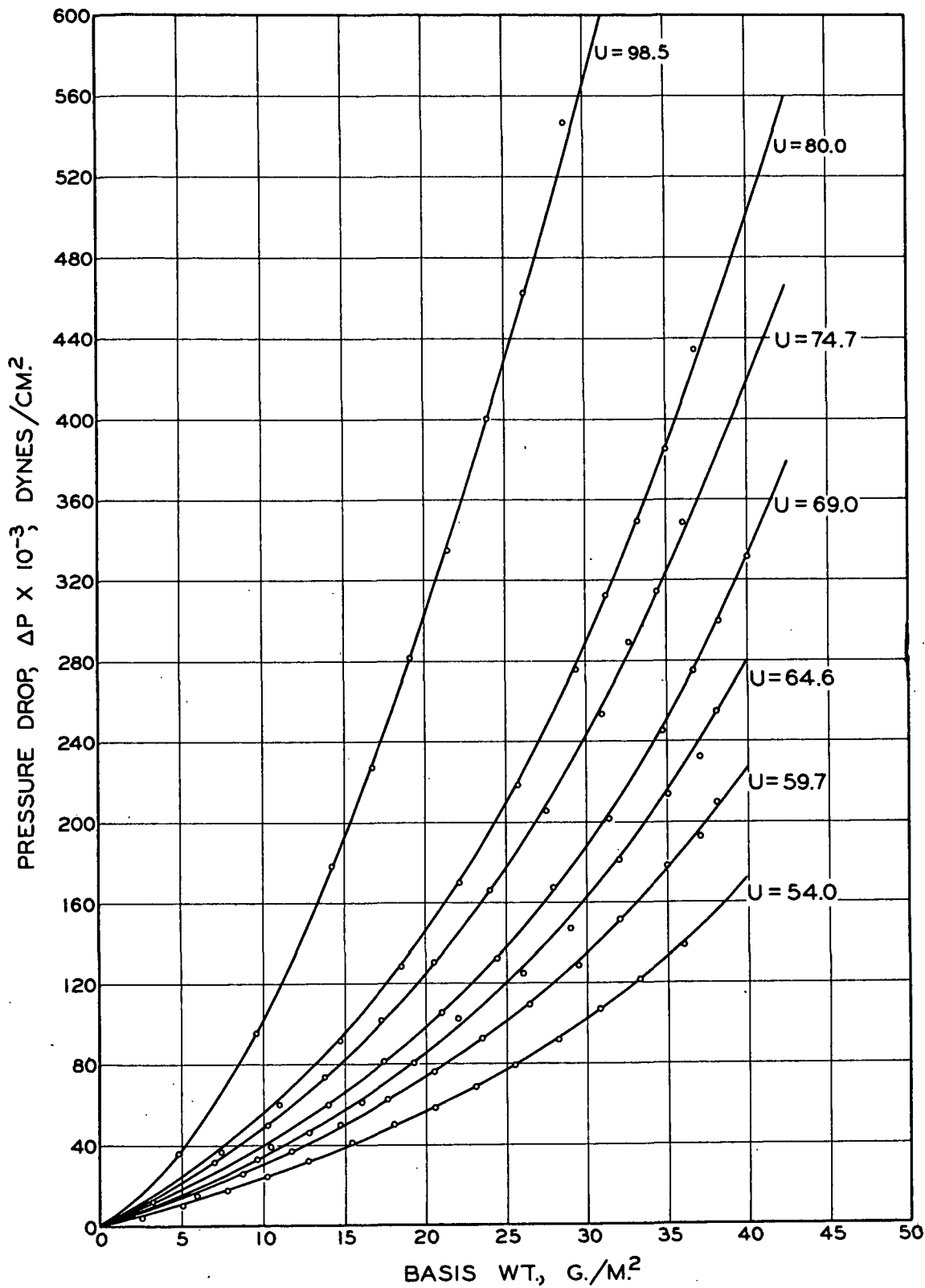


Figure 13. Dynamic Drainage Tester Run Data of Wood Pulp. Mat Pressure Drop, ΔP , as a Function of Superficial Velocity, \underline{U} , and Basis Weight (Mats on 65-Mesh Wire; Higher Velocity Range)

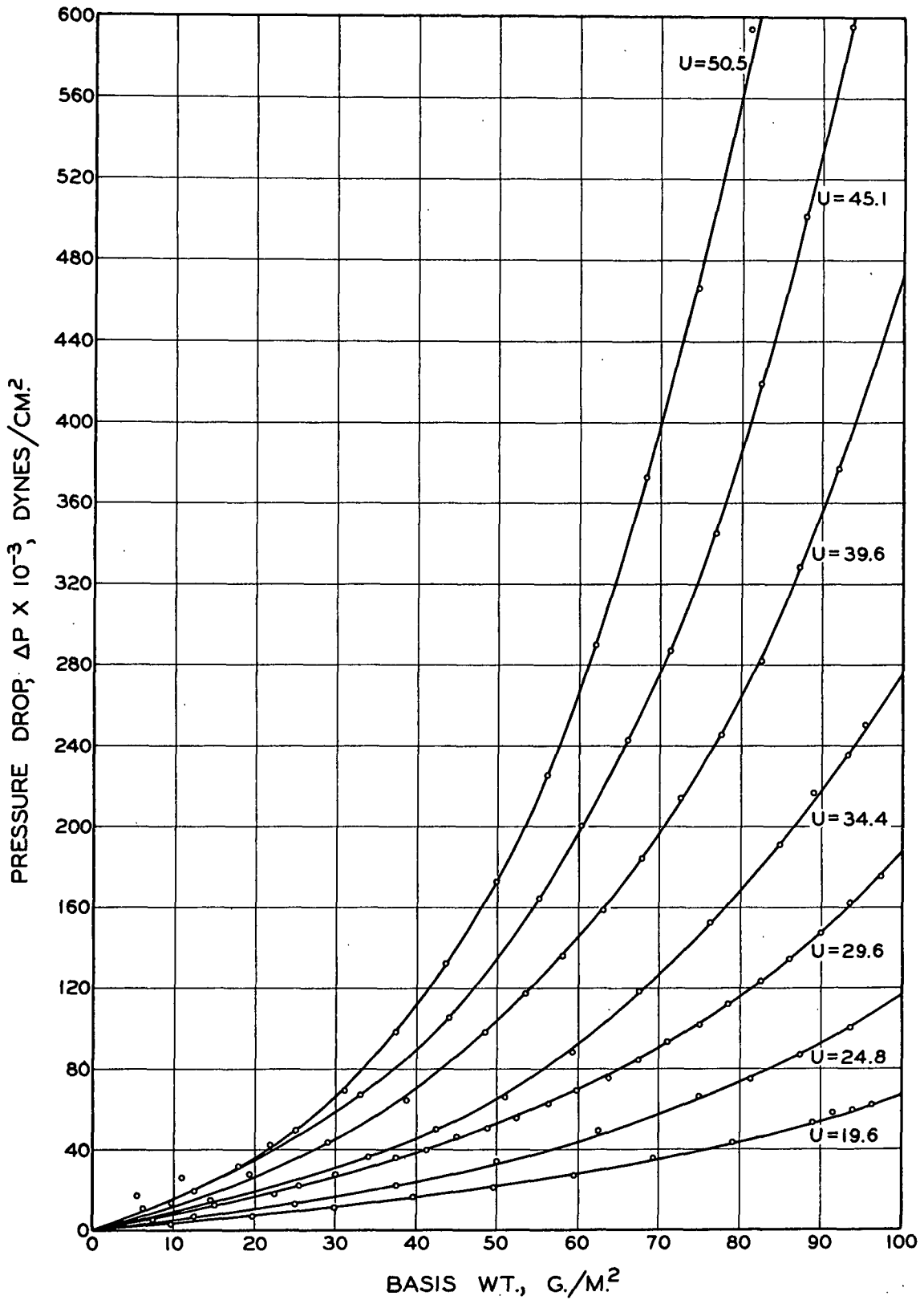


Figure 14. Dynamic Drainage Tester Run Data of Wood Pulp. Mat Pressure Drop, ΔP , as a Function of Superficial Velocity, U , and Basis Weight (Mats on 100-Mesh Wire; Lower Velocity Range)

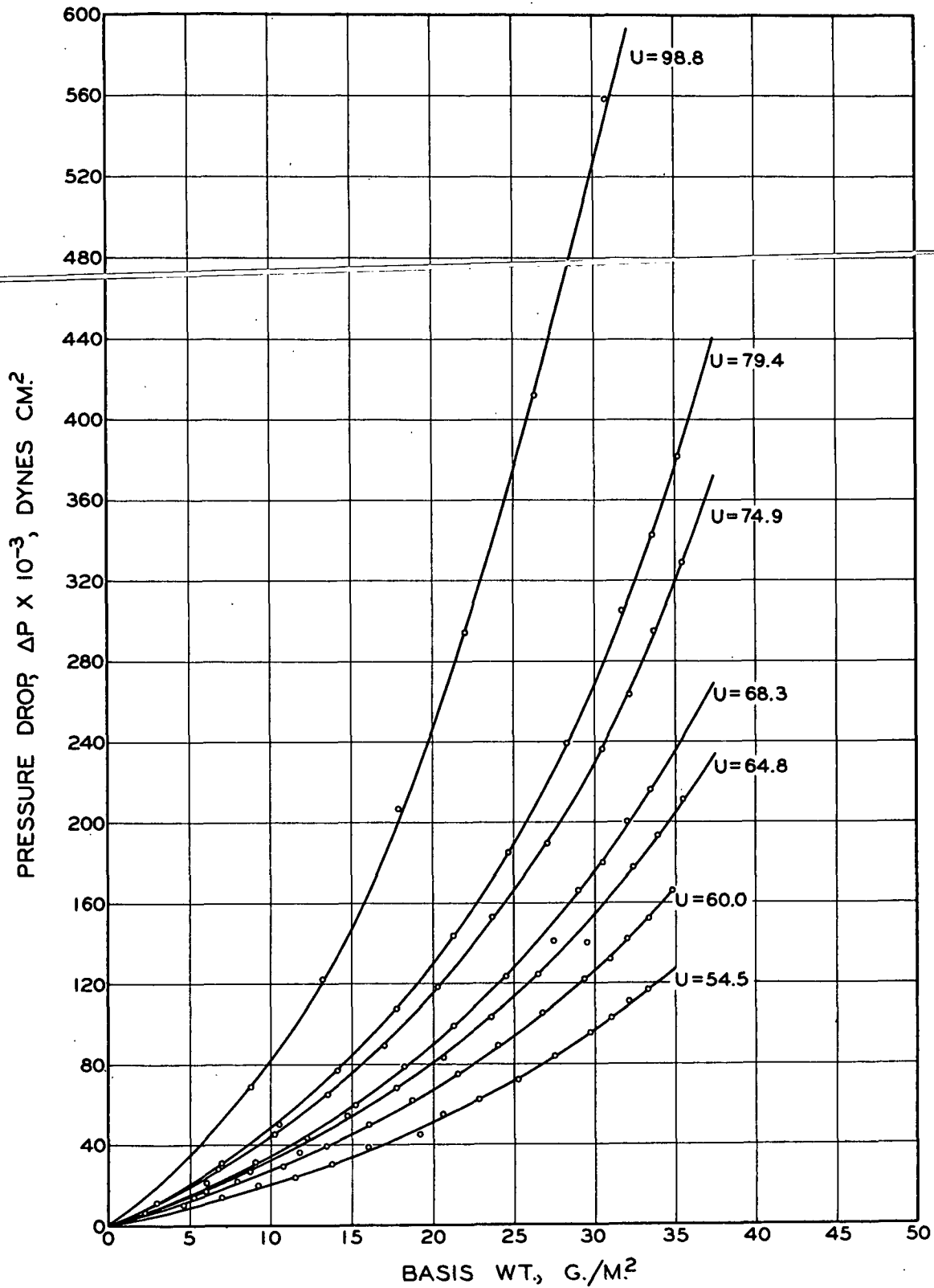


Figure 15. Dynamic Drainage Tester Run Data of Wood Pulp. Mat Pressure Drop, ΔP , as a Function of Superficial Velocity, U , and Basis Weight (Mats on 100-Mesh Wire; Higher Velocity Range)

IPST HASLTON LIBRARY



5 0602 01065011 9